

# QUILL

## Quarterly Reports



November 21 – January 22



All information held within is confidential and is

Copyright © QUILL 2022.

It contains proprietary information which is disclosed for information purposes only.

The contents shall not in whole or in part

(i) be used for other purposes,

(ii) be disclosed to any person not being a member of staff or student of QUILL

(3 year period up to February 2025)

(iii) be disclosed to any person not being a member of staff of a QUILL industry member or one of their affiliated companies,

(iv) be stored in any retrieval system, or reproduced in any manner which does not fulfil conditions (i), (ii) and (iii) without the written permission of the Director of QUILL, The Queen's University of Belfast, David Keir Building, Stranmillis Road, Belfast BT9 5AG, United Kingdom.



## Contents

Design of New, Non-coordinating, and Hydrophobic Anions for Functional Ionic Liquids (Haris Amir).....	4
Recycle and Reuse of Process Water Through Sulfate Removal: Developing an Ionic Liquid Technology for Selective Anion Recognition and Extraction (Dominic Burns) .....	10
Battery Thermal Management and Algorithmic 3D Temperature Prediction (Andrew Forde) .....	14
Mechanism Understanding of NO <sub>x</sub> storage, release and reduction on Pt/doped ceria catalysts (Oisin Hamill).....	15
Intrinsically Ionic Liquid Catalytically Active Frustrated Lewis Pairs (Aloisia King).....	17
Design of supported ionic liquid catalysts for the synthesis of 5-substituted tetrazoles to be used as draw fluids for forward osmosis in water desalination (Sanskrita Madhukailya) .....	19
Design and Development of an Effective and Interconnected Smart Fire Suppression System for Lithium-ion Batteries in Electric Vehicles (David McAreavey).....	21
Chemisorbent materials for olefin and paraffin separation (Sam McCalmont).....	23
Valorisation of Waste Polyolefin Plastics Using Lewis Acidic Ionic Liquids (Emma McCrea) .....	26
Boron Lewis acids: structure and applications (Anne McGrogan).....	28
Thinking inside the (glove)box: Lewis Superacidic Ionic Liquids Based on Main Group Cations (Shannon McLaughlin) .....	30
Redox Flow Battery Materials for Energy Storage (Hugh O'Connor) .....	35
3D-printed polymer graphene nanocomposites for biosensor applications (Liam O'Connor) .....	37
Molecular Electrocatalysts for Energy and Electrosynthetic Applications (Scott Place) .....	38
Use ionic liquids that exhibit LCST (lower critical solution temperature) behaviour as draw fluids for water treatment, desalination and separation (Junzhe Quan).....	40
Thermochemical Conversion of Biomass Lignin into Mesoporous Carbon Materials (Yaoguang Song) .....	44
Modelling the use of Flow Batteries in Transport Applications (Richard Woodfield).....	52
Gas separation technologies (Mark Young).....	53

## QUILL Quarterly Report

November 2021 – January 2022

<b>Name:</b>	Haris Amir		
<b>Supervisor(s):</b>	Professor John Holbrey		
<b>Position:</b>	Postgraduate (PhD)		
<b>Start date:</b>	1/10/2020	<b>Anticipated end date:</b>	30/09/2023
<b>Funding body:</b>	ESPRC/UKRI		

### Design of New, Non-coordinating, and Hydrophobic Anions for Functional Ionic Liquids

New boron containing anions are of interest for the development of new ionic liquid anions with a wide range of potential applications including electro- and photo- chemistry, and for the separation and extraction of metals and waste. In this work, functional borate anions formed as complexes with O/N-chelators for ionic liquid applications have been designed and investigated.

It is known ortho-borate anions have a high tendency to undergo hydrolysis, in the presence of only trace amounts of water. The stability of new boron containing anions in the presence of water has been examined through assessment of the impact of the boron-coordination environment on the coordinative stabilities of borate anions incorporating common O- and unique N/O- donor ligands (figure 1) in the form of alkali salts *via* NMR spectroscopy. Anion exchange with tetrabutylphosphonium chloride [P<sub>4444</sub>]<sup>+</sup>Cl<sup>-</sup> has been used to obtain ionic liquids with [P<sub>4444</sub>]<sup>+</sup> cations combined with the different borate anions, forming ionic liquids that have been chemically and physically characterised (including thermal stability and decomposition). In addition, in several cases tetrabutylphosphonium borate salts were also obtained, with melting points above room temperature, that could be isolated as crystals allowing single crystal XRD studies to be performed showing cation-anion packing motifs and hydrogen-bonding in the solid state and also, critically, confirming the four-coordinate, anionic nature of the boron-containing species.

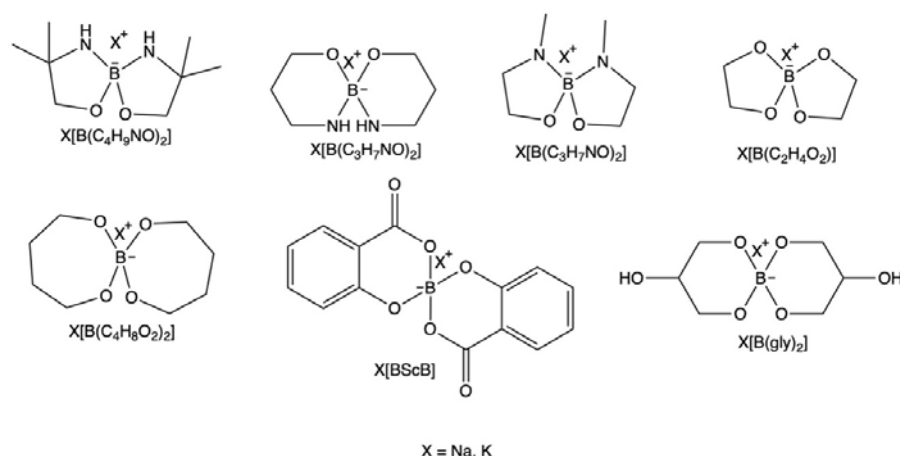


**Figure 1** - Structure of the orthoborate anions under investigation with B{OOOO} and B{OONN} coordination environments

## Stability in D<sub>2</sub>O

Ortho-borate anions containing B-O bonds are prone to hydrolysis even with minimal amounts of water, as B-O bonds are labile. Therefore, alkali salts of the borate anions illustrated in figure 1 was dissolved in D<sub>2</sub>O and the hydrolytic stability of the 4-coordinate borate-centre was investigated using <sup>11</sup>B NMR spectroscopy. It was found that the familiar tetra-oxo (B{OOOO}) coordination environment undergoes hydrolytic dissociation as expected, as shown by a decrease in the peak centred around 3 ppm (four-coordinate boron) and the emergence of a new peak at 10 ppm (characteristic of three-coordinate boron) illustrating how labile B-O bonds are in the presence of water. In contrast, with borate anions containing the mixed oxygen/nitrogen coordination environment, no decomposition of the anion was observed on dissolution in water. An example of this is shown in figure 2 for the anion [B(C<sub>4</sub>H<sub>9</sub>NO)<sub>2</sub>]<sup>-</sup> (top left in figure 1) where the light blue line shows the <sup>11</sup>B NMR signal 1 hour after the addition of water and the red line shows the spectrum after one week with now change in the chemical shift of the <sup>11</sup>B NMR signal.

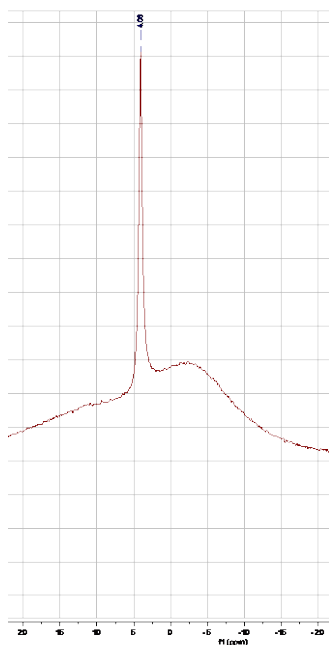


**Figure 2** - <sup>11</sup>B NMR of Na[B(C<sub>4</sub>H<sub>9</sub>NO)<sub>2</sub>] in D<sub>2</sub>O (red: after 1-week, light blue: 1 hour). Note, the broad baselines are due to the presence of boron in borosilicate glass NMR tubes

As shown in the spectra the mixed oxygen/nitrogen borate anions are seen to be stable in the presence of water and do not undergo hydrolysis to form three-coordinate neutral species. From this investigation it can be anticipated that tetra-azo borate anions (B{NNNN} coordination) that are a target for the next stage of work, will also be exceptionally robust and stable to hydrolysis.

## Crystal Data

Detailed analysis of the crystallographic data obtained from single crystal XRD studies on tetrabutylphosphonium borate salts obtained with the B{OOOO} and B{OONN} coordination environments is ongoing. Currently the structures of tetrabutylphosphonium salts with the following anions [B(C<sub>3</sub>H<sub>7</sub>NO)<sub>2</sub>]<sup>-</sup>, [B(gly)<sub>2</sub>]<sup>-</sup> and [BScB]<sup>-</sup> has been analysed, showing the coordination and connectivities of the ions present in the crystals as expected. The crystal structure ion-pair connectivities and respective unit cells are shown below.

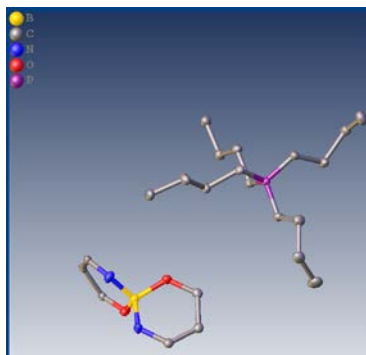


**Figure 3a** - Crystal structure of  $[P_{4444}][B(C_3H_7NO)_2]$

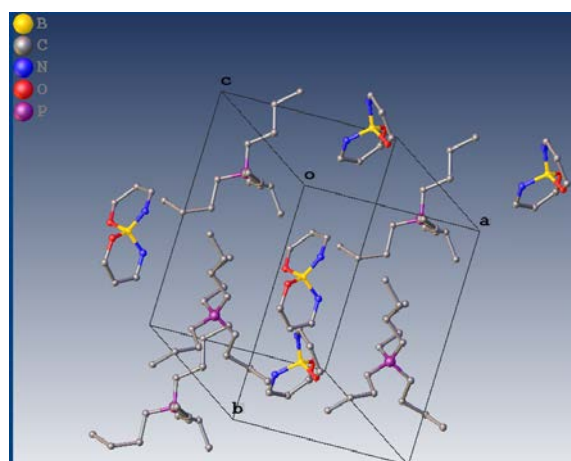


**Figure 3b** - Unit cell of  $[P_{4444}][B(C_3H_7NO)_2]$

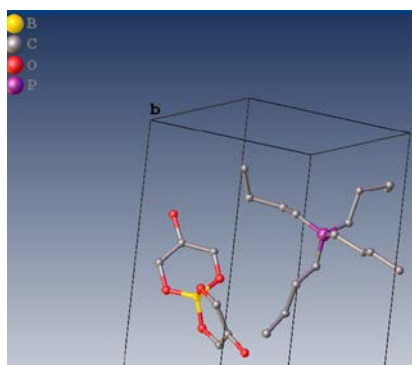


**Figure 4a** - Crystal structure of  $[P_{4444}][B(gly)_2]$

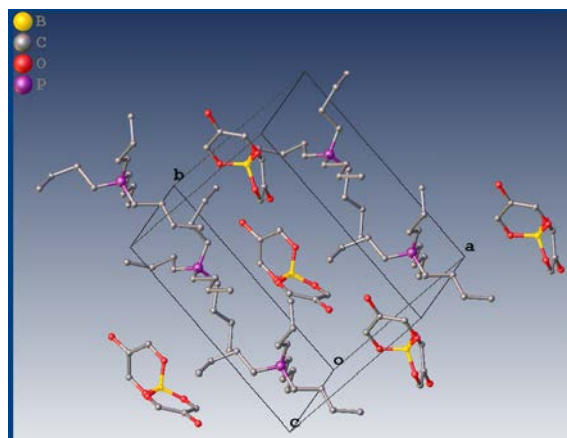


**Figure 4b** - Unit cell of  $[P_{4444}][B(gly)_2]$

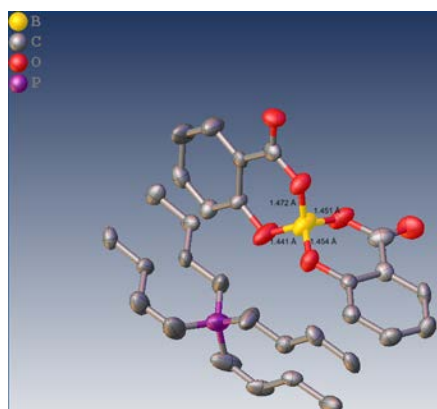


**Figure 5a** - Crystal structure of  $[P_{4444}][BScB]$

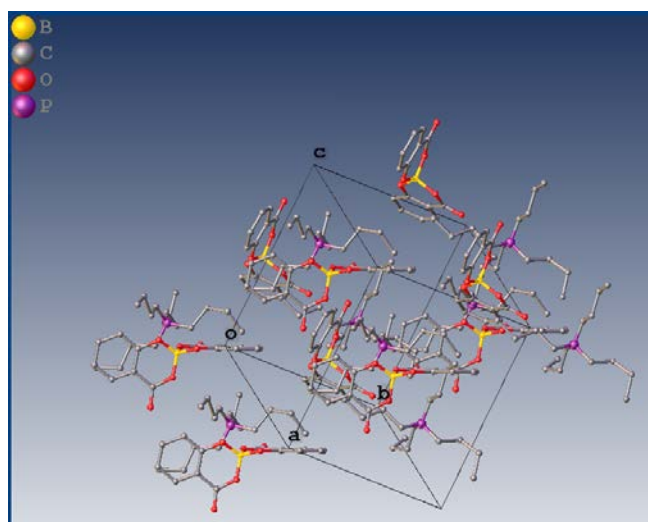


**Figure 5b** - Unit cell of  $[P_{4444}][BScB]$

Similar cation conformations and packing is observed in the unit cells of each of the structures shown here, with alternate layers of cations and anion stacked on top of one another, this was as

predicted when it comes to the unit cell of ionic liquids. The layers are likely held together with hydrogen binding, this will be further investigated upon further crystallographic analysis.

### Thermogravimetric Analysis (TGA)

Dynamic thermogravimetric analysis (TGA) was used to study the thermal stability and decomposition pathways of the ionic liquids synthesised. The percentage of the mass loss upon gradual heating ( $2^{\circ}\text{C}/\text{min}$ ) of the samples was used as a method of describing the thermal stability of these products. Initially all the samples were prepared by using a standard platinum pan, as a result the samples could be heated to  $900^{\circ}\text{C}$ .  $[\text{P}_{4444}][\text{BScB}]$ , containing (salicylato)borate anions, rapidly decomposes in two concerted steps between  $300$  and  $350^{\circ}\text{C}$ , with complete mass loss over this region. In contrast,  $[\text{P}_{4444}][\text{B}(\text{C}_3\text{H}_7\text{NO})_2]$ , although showing small mass losses from  $100$ - $200^{\circ}\text{C}$  (likely moisture and/or other partially volatile contaminants) has a greater thermodynamic stability and undergoes a first mass loss even from *ca.*  $350^{\circ}\text{C}$  (16% mass) followed by 70% mass loss between  $450$  and  $600^{\circ}\text{C}$  with the inflection point around  $550^{\circ}\text{C}$  (endset temperature of  $589^{\circ}\text{C}$ ). From the NMR and TGA study currently completed, the introduction of B-N bonds improves the stability of 4-coordinated borate anions in the presence of water, as well as significantly improving the thermodynamic stability of  $[\text{P}_{4444}]^+$  based ionic liquids.

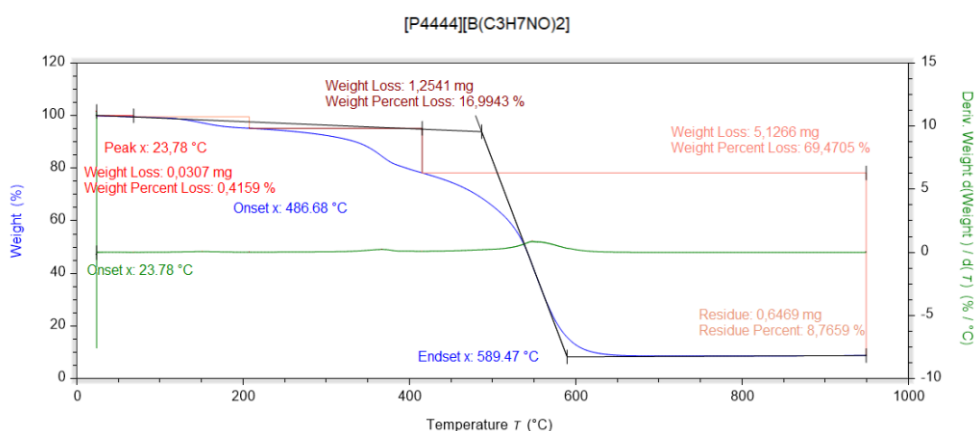


Figure 6 - TGA curve of  $[\text{P}_{4444}][\text{B}(\text{C}_3\text{H}_7\text{NO})_2]$ , Pt-pans, heating at  $2^{\circ}\text{C}/\text{min}$

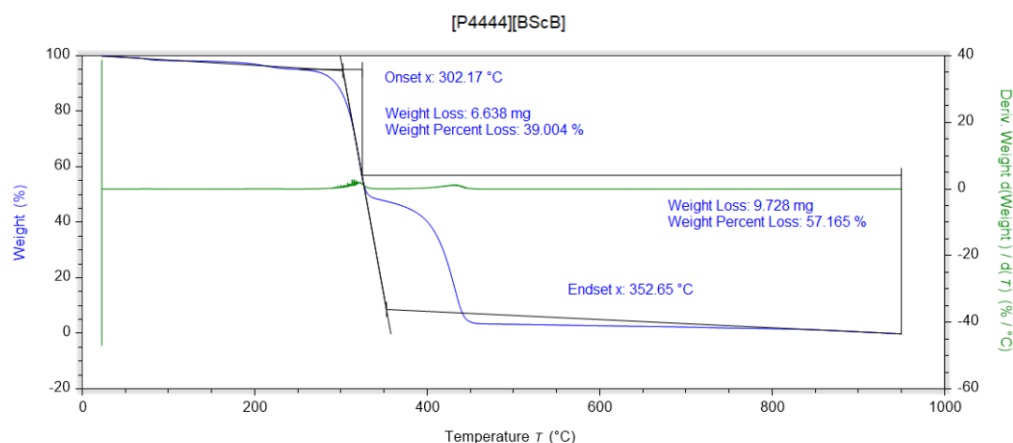


Figure 7 - TGA curve of  $[\text{P}_{4444}][\text{BScB}]$ , Pt-pans, heating at  $2^{\circ}\text{C}/\text{min}$





### **Future work**

Future work will be to complete thermophysical characterisation of trihexyltetradecylphosphonium  $[P_{66614}]^+$  ionic liquids generated with these new borate anions, including density and viscosity characterisation, and the data compared with that of known  $[P_{66614}]^+$  ionic liquids from the literature. TGA will be gathered on the remaining  $[P_{4444}]^+$  ionic liquids as well as differential scanning calorimetry (DSC), to obtain the glass transition point of the ionic liquids. As well as the remaining XRD data on the crystals of the ionic liquids synthesised.

Having identified interesting, hydrolytically stable  $B\{OONN\}$  anion motifs, corresponding  $B\{NNNN\}$  coordination environments will be investigated and ionic liquid materials generated for further study.

## QUILL Quarterly Report

November 2021 – January 2022

<b>Name:</b>	Dominic Burns		
<b>Supervisor(s):</b>	Prof John Holbrey, Prof Gosia Swadzba-Kwasny and Dr Hye-Kyung Timken		
<b>Position:</b>	PhD Student		
<b>Start date:</b>	1 <sup>st</sup> October 2019	<b>Anticipated end date:</b>	30 <sup>st</sup> September 2023
<b>Funding body:</b>	EPSRC		

### Recycle and Reuse of Process Water Through Sulfate Removal: Developing an Ionic Liquid Technology for Selective Anion Recognition and Extraction

#### Background

This is an EPSRC industrial CASE project in collaboration with Chevron, to explore technologies for the treatment of saline process water with the initial objective of selective sulfate removal from highly competitive aqueous streams. Extraction of hydrophilic oxyanions from aqueous solutions is an important industrial challenge across many sectors, from acid mine drainage to nuclear waste remediation, nuclear medicine, and general water treatment to address compliance with total discharge limits. Previously examined was the applicability of hydrophobic ionic liquid media for liquid-liquid extraction of a range of oxyanions from non-competitive aqueous solutions. It has been demonstrated that sulfate anions ( $[\text{SO}_4]^{2-}$ ), can be extracted from 27.1 mM aqueous solutions with 57% efficiency using  $[\text{P}_{66614}]\text{Cl}$ , also known as CYPHOS<sup>®</sup> IL 101. A 2:1 chloride:sulfate anion exchange mechanism is found to overcome the Hofmeister series; however, this is strongly inhibited by excess chloride concentrations, for example from brine solutions.

The current main approach is a liquid-liquid extraction where anion receptors such as **1** (in Fig. 1) are dissolved into the IL phase which can then bind to the sulfate and stabilise it in the IL phase. Another approach currently being investigated is possibility of building a covalent organic framework (COF) based on tetraphenyladamantane nodes with diaminoguanidine hydrochloride linkers. The diiminoguanidinium moiety has been extensively shown in the literature to strongly bind sulfate [1].

#### Objective of this work

The main goal of this work is the selective removal of sulfate from sea water with a lesser emphasis on removal of sulfate from other competitive aqueous streams. A secondary goal of the research is to develop methods for the removal of toxic or valuable oxyanions of interest from water streams such as naphthenic acids, phosphates ( $[\text{H}_x\text{PO}_4]^{y-}$ ), nitrate ( $[\text{NO}_3]^-$ ), bromate ( $[\text{BrO}_3]^-$ ), arsenates ( $[\text{H}_x\text{AsO}_4]^{y-}$ ), pertechnetate ( $[\text{TcO}_4]^-$ ), chromate ( $[\text{CrO}_4]^-$ ) and selenate ( $[\text{SeO}_4]^{2-}$ ) [2,3].

#### Progress to date

This quarter mainly focused on completion of validation of results previously obtained and reported. To briefly summarise some of it, extractions with neat  $[\text{P}_{66614}]\text{Cl}$  were expanded upon and other anions such as  $[\text{HSO}_4]^-$ ,  $[\text{PO}_4]^{3-}$ ,  $[\text{MnO}_4]^-$  and  $[\text{BrO}_3]^-$  were extracted in a similar fashion to sulfate. The results are shown in figure 1 and clearly indicate that extraction is dependent on the

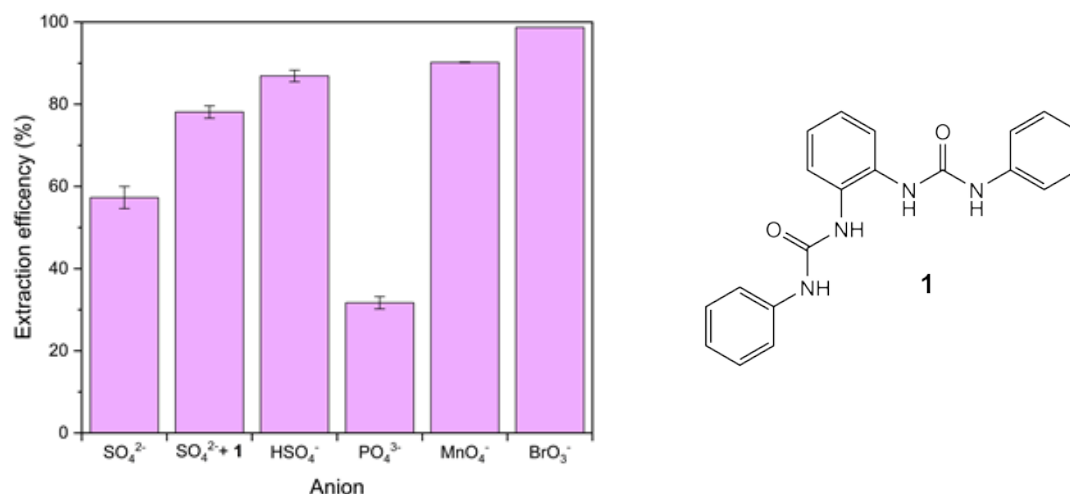


**Figure 1** - Extraction efficiency of anions from 27.1 mM solutions added as sodium salts, extracted into a neat  $[\text{P}_{66614}]\text{Cl}$  phase (left).  $[\text{SO}_4]^{2-} + \mathbf{1}$  shows the improved extraction upon the addition of 2 equivalents of receptor **1** (right). \* $[\text{MnO}_4]^-$  added as potassium salt and extracted from a 10 mM solution.

hydrophilicity of the target anion, with monovalent anions extracted in greater quantities than their di and tri-valent counterparts.

On development of the adamantane-based COF, proposed as a solid sulfate-selective binder, the synthetic route to the proposed adamantane-guanidinium COF is shown in figure 2. Although each step in the sequence appears relatively straightforward, there are a number of challenges with the purification stages that have to be addressed to complete this material. The first product,

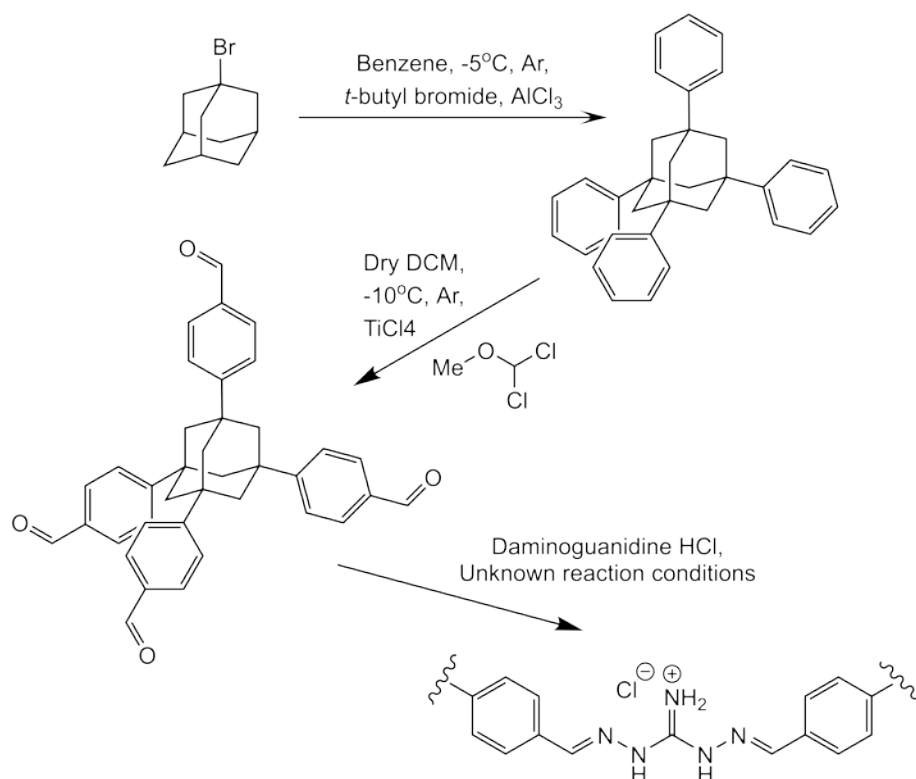


**Figure 2** - Synthetic route to the relatively common COF structural sub-unit TFPA and how these moieties may be linked together via diiminoguanidinium chloride bridges.

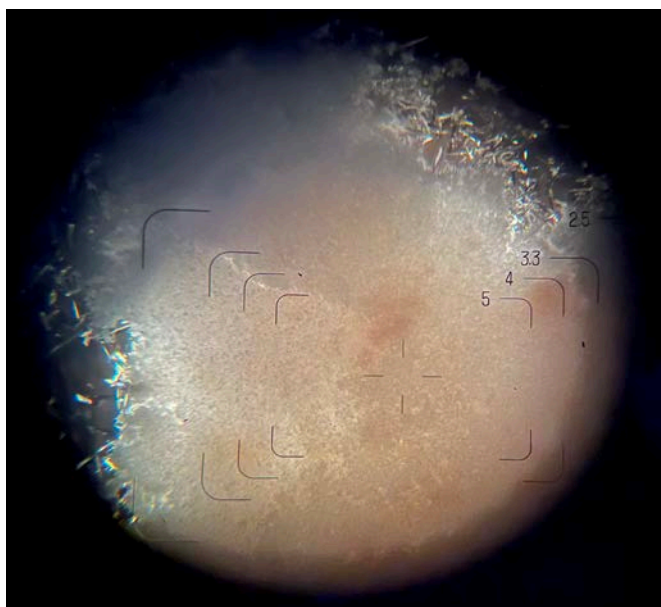


**Figure 3** - Thermal annealing of the tetraphenyladamantane above 200°C.

tetraphenyladamantane (TPA), is entirely insoluble in all common organic solvents and so can easily be separated from starting materials as well as the mono, bi and tri, phenylated intermediates. Interestingly, while determining the melting point of tetraphenyladamantane on a hot-stage microscope, thermal annealing could be observed above 200°C as the edges of the sample began to crystallise. A photograph of this is included in figure 3. Formylation of tetraphenyladamantane to produce 1,3,5,7-tetrakis(4-formylphenyl)adamantane (TFPA) was then undertaken to generate reactive aldehyde groups for subsequent condensation with diaminoguanidine. This material has been successfully synthesised, however additional purification is required before it can be used to for the synthesis of the desired COF, as minor impurities are present as seen in the  $^1\text{H}$  NMR spectrum shown in figure 4.

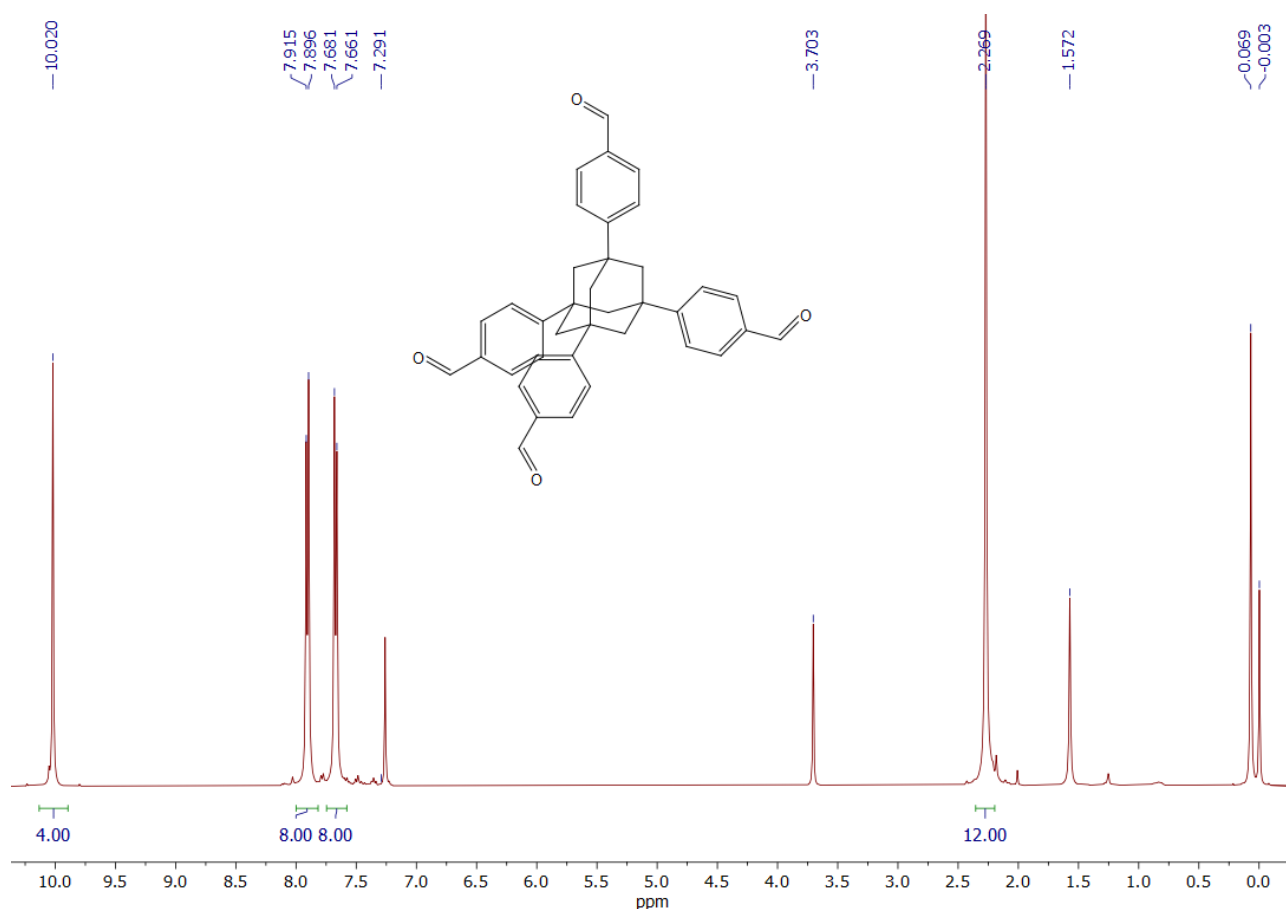


**Figure 4** -  $^1\text{H}$  NMR of the crude TFPA product.

### Conclusions and future work

To summarise, the hydrophobic phosphonium ionic liquid [P<sub>66614</sub>]Cl has been shown to be an anion exchanger enabling a range of undesirable oxyanions to be extracted from aqueous solutions with moderate to good extraction efficiency. The addition of various anion receptors, notably **1**, can improve the extraction efficiency, however, this still not enough for real world applications and is inhibited by the presence of excess monovalent hydrophilic anions such as chloride present in typical saline streams. The synthesis of a proposed adamantane-guanidinium COF is well underway although is it still far too early to draw any conclusions about this approach.

### References

1. R. Custelcean, *Chem. Commun.*, 2020, **56**, 10272–10280.
2. L. N. Pincus, H. E. Rudel, P. V. Petrović, S. Gupta, P. Westerhoff, C. L. Muhich and J. B. Zimmerman, *Environ. Sci. Technol.*, 2020, **54**, 9769–9790.
3. J. R. E. Jones, *J. Exp. Biol.*, 1941, **18**, 170–181.



## QUILL Quarterly Report

November 2021 – January 2022

<b>Name:</b>	Andrew Forde		
<b>Supervisor(s):</b>	Dr Stephen Glover, Dr Rob Watson and Prof Peter Nockemann		
<b>Position:</b>	PhD Student		
<b>Start date:</b>	03/06/2019	<b>Anticipated end date:</b>	03/12/22
<b>Funding body:</b>	Horiba-MIRA & EPSRC		

### Battery Thermal Management and Algorithmic 3D Temperature Prediction

#### Experimental

A collaboration has been established with University College London. Work has been carried out in the battery group of UCL involving acoustic measurements for monitoring of SOC and temperature. As this project is interested in internal battery temperature, these methods are well suited for model parameterisation and validation.

The commercial cells to be used for this project were sent to UCL for acoustic measurements. These measurements have now been taken. Safety precautions for use and storage of these cells at QUB have been discussed and transport is being organised to move the cells to QUB for the remainder of the experimental work.

Tests for battery safety are being investigated and designed after issues were raised with an initial plan of using gas chromatography. This method would not achieve the accuracy required to be certain of safety so is currently being altered to achieve these requirements

#### Numerical Model

A 3D conduction model has been developed to allow for parameterisation of the thermal model following experimental work. This will use a uniform heat source on one face of the cell to determine thermal conductivities of various regions throughout the cell

## QUILL Quarterly Report

November 2021 – January 2022

<b>Name:</b>	Oisin Hamill		
<b>Supervisor(s):</b>	Dr Nancy Artioli and Dr Alex Goguet		
<b>Position:</b>	PhD		
<b>Start date:</b>	01/10/2019	Anticipated end date:	30/03/2023
<b>Funding body:</b>	EPSRC		

### Mechanism Understanding of NO<sub>x</sub> storage, release and reduction on Pt/doped ceria catalysts

#### Background

Due to strengthening emission legislations in Europe, North America and the rest of the world, there is a need for further optimisation of existing emission after-treatment catalytic converters for automotive applications. New legislations focus primarily of NO<sub>x</sub> abatement and consequently the exhaust emissions of lean-burn gasoline and diesel vehicles. After treatments systems must utilise new technologies to reduce this that offer low temperature activation and high stability.

High surface area ceria is successfully employed as an excellent support of metals (Pd, Rh, Pt, etc.) in commercial catalytic systems for the oxidations of carbon monoxide and propane and automotive emission control. Ceria is a unique material with a rich and complex chemistry. It possesses high oxygen storage capacity (OSC), a unique redox property by the cycle of Ce<sup>4+</sup>/Ce<sup>3+</sup> redox pairs and it can be further enhanced through using dopants. Platinum supported on ceria can show enhanced NO<sub>x</sub> storage at low temperature, as reported in the literature, together with an improved carbon monoxide/hydrocarbon light off.

Ceria supported catalysts, in general, do not operate efficiently at low temperatures and therefore must be modified in order to overcome this problem. For this reason, addition of enhancing materials is currently being considered in detail. This addition of a material that increases the performance of an already functional catalyst is called doping. The main function of this dopant is to allow the catalyst to function outside of the normal working temperature range and operating conditions to increase catalyst efficiency.

It has been proposed that the dopants, such as rare-earth and transition metal oxides, increase the concentration of surface vacancies which affect the ionic conductivity, oxygen mobility and oxygen storage capacity of the ceria. It can be speculated that all these properties are responsible for the enhanced oxidation activity by promoting oxygen diffusion and formation of more "reactive oxygen" species. Furthermore, the oxygen species play a role in the mechanism of the reaction, favouring the NO<sub>x</sub> storage.

Additionally, presence of dopants can reportedly modify the platinum reducibility and platinum-ceria interaction, allowing more readily activation during rich purge.

This project aims to better understand the NO<sub>x</sub> storage mechanism on the doped materials and give new insights into the activation/lean deactivation mechanisms in the presence of different dopants.



### **Objective of this work**

The main objective considered in this project is to improve the understanding of the NO<sub>x</sub> storage mechanism, together with the mechanism of rich purge on ceria supported platinum. We aim to gain a deeper knowledge of the rich activation and lean deactivation mechanisms as well as determine the structure of the active sites under reaction conditions. We look to develop a method to differentiate between active species and spectator species through transient methods. We will also strive to develop a global kinetic model for the reaction and all involved species. This will enable the determination of the relative importance of different reactions within the catalyst bed as well as a measurement of the exact gas compositional conditions present during the reactions. With this approach in depth information relevant to mechanistic understanding and reaction engineering application will be obtained.

### **Progress to date**

- Characterisations for dopant oxides completed.
- Characterisations for Sm-Al catalysts completed.
- NSC on Sm-doped catalysts completed.
- NSC for other dopants started.
- NAM27 oral abstract accepted & presentation structure discussed.
- UKCC presentation shown at conference in Jan.

### **Conclusions and future work**

- Complete activation tests on new Sm-Al family of catalysts.
- Complete activation tests on Pr and other dopants families.
- Complete dopant oxide characterisations.
- Submit in-situ & ex-situ EXAFS proposal for diamond.
- Complete XPS for all catalysts.
- Complete H<sub>2</sub> chemisorption experiments to determine Pt dispersion.
- TEM & EELS results to be returned and analysed.



## QUILL Quarterly Report

November 2021 – January 2022

<b>Name:</b>	Aloisia King		
<b>Supervisor(s):</b>	Prof John Holbrey and Prof Małgorzata Swadźba-Kwaśny		
<b>Position:</b>	PhD student		
<b>Start date:</b>	01 Oct 2020	<b>Anticipated end date:</b>	03 March 2024
<b>Funding body:</b>	EPSRC		

### Intrinsically Ionic Liquid Catalytically Active Frustrated Lewis Pairs

#### Background

Frustrated Lewis acid/base pairs (FLPs) have emerged as potential metal-free alternatives to platinum group metal catalysts. Typical examples are combinations of a sterically hindered bulky phosphine Lewis base with a strongly electrophilic borane Lewis acid. FLPs have been shown to activate hydrogen, serving as metal-free hydrogenation catalysts [1]. While many of the advances in FLP chemistry have sought to exploit these bulky phosphine/borane pairs, less attention has been given to purely organic systems, although examples with non-boron Lewis acid FLP components are known including N-alkylacridinium cations which form FLPs with lutidine as a base [2].

#### Objective of this work

The goal of this research is to develop organic-based FLPs within an intrinsic IL media. There are copious amounts of research carried out on FLPs and even an example of FLP in IL media. However, not much attention has been given to organic-based FLPs in an intrinsic IL media. The main aim is to create FLPs within ILs that can replace a catalyst in a range of reactions and hence, ultimately replace conventional solvents. Therefore, creating greener and more affordable chemistry through facile synthesis.

#### Progress to date

The ability to extend the lifetimes of FLP encounter complexes by dissolution of the Lewis acid and base components into IL environments enabling detection on the NMR timescale in solution has previously been demonstrated from research conducted within QUILL [3]. Recognizing that the  $H^+/H^-$  pairs formed by heterolytically splitting hydrogen ( $H-H$ ) by a phosphine/borane FLP can be stabilized as protonated-phosphonium/hydridoborate ion pairs, we reasoned that an intrinsic FLP forming composite ionic liquid, that would be catalytically active for a range of small molecule ( $H_2/CO_2$  etc.) activation, could be generated by combining acridinium salts into a base-rich protic lutidinium ionic liquid enabling the  $H_2$  activation within the buffered ionic liquid through the reaction shown in figure 1.

To date, I have successfully synthesized two ILs that will be the media to dissolve and study the activity of acridinium and other Lewis acidic organic heterocyclic cations, and of which will form the bases of a buffered ionic liquid base component of the intrinsically ionic liquid FLP. The ILs that have been made and fully characterized are [H-lutidinium] [NTf<sub>2</sub>] and [H-picolinium] [NTf<sub>2</sub>]. Additionally, I investigated a number of methods from the literature to successfully alkylate sterically hindered acridine to generate N-alkylacridinium salts. Through optimization of these methods the following salts were synthesized and fully characterized; 10-butyl acridinium bromide, 10-methyl-acridinium methyl sulfate and 10-ethyl-acridinium bromide. The initial acridinium methyl sulfate and bromide

salts were subjected to an anion-exchange reaction with  $\text{Li}[\text{NTf}_2]$  to form the bis(trifluoromethyl)sulfonylimide salts; [methylacridinium][ $\text{NTf}_2$ ], [ethylacridinium][ $\text{NTf}_2$ ], and [butylacridinium][ $\text{NTf}_2$ ]. The solubility of these salts was tested in the lutinium and picolinium ILs and all the salts were soluble within these IL media.

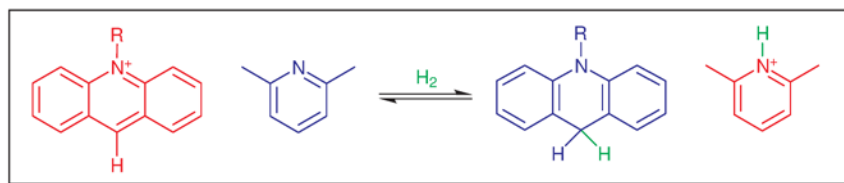


**Figure 1** - Proposed FLP activation of  $\text{H}_2$  through heterolytic cleavage at a N-alkylacridinium cation/lutidine FLP buffered in lutidine/[H-lutidinium] $^+$  protic ionic liquid forming N-alkyl-9,10-dihydroacridine and a H-lutidinium cation.

### Conclusions and future work

I have submitted an abstract for the EUCHEMSIL conference in June, including in my abstract the information provided throughout this report. Full chemical and thermophysical characterisation of the ILs and organic salt precursors synthesised will be conducted on both the new IL materials and on protic Lutidinium systems to address the limited characterisation information currently within the literature. It is notable that the acridinium salts generated are fluorescent, and their optical and fluorescence behaviour will be determined. Acridine, the initial target for generating IL-like cationic Lewis Acid FLP components is particularly challenging to N-alkylate due to the combination of electron-delocalisation and steric hindrance that is imposed on the molecule, due to the cyclic ring systems on either side. Further optimisation of alkylation approaches will be conducted to broaden the scope and range of cationic Lewis acids available for study. Additionally, to extend the scope for Lewis acid targets, 3, 5-disubstituted 1, 4-dihydropyridines will be investigated for their potential as the cation constituent to complement the acridinium species. This idea stemmed from the fact that these molecules are reported to have a similar hydride-donating ability to the acridinium species [4]. Characterisation and screening of the intrinsic IL FLPs will be initiated, using  $^1\text{H}$  NMR analysis to follow the equilibrium as shown in Fig 1 on addition of  $\text{H}_2$  gas (4 bar, mapping to the literature [2] in conventional solvents).

### References

1. D. W. Stephan and G. Erker, *Angew. Chem. Int. Ed.*, 2010, 49, 46–76.
2. E. R. Clark and M. J. Ingleson, *Angew. Chem., Int. Ed.*, 2014, 53, 11306–11309.
3. L. C. Brown, S. Gaertner, J. D. Holbrey, J. M. Hogg, M. Gilmore, L. Moura, S. Imberti, H. Q. N. Gunaratne, R. J. O'Donnell, N. Artioli and M. Swadzba-Kwasny, *Chem. Commun.*, 2018, 54, 8689–8692.
4. H. Zhao, Y. Li and X. Zhu. *ACS Omega*. 2018, 3 (10), 13598–13608.

## QUILL Quarterly Report

November 2021 – January 2022

<b>Name:</b>	Sanskrita Madhukailya		
<b>Supervisor(s):</b>	Professor John Holbrey and Dr. Leila Moura		
<b>Position:</b>	PhD Student (First year)		
<b>Start date:</b>	19 <sup>th</sup> April 2021	<b>Anticipated end date:</b>	20 <sup>th</sup> April 2024
<b>Funding body:</b>	Tezpur University/QUB joint PhD scholarship		

### Design of supported ionic liquid catalysts for the synthesis of 5-substituted tetrazoles to be used as draw fluids for forward osmosis in water desalination

#### Background

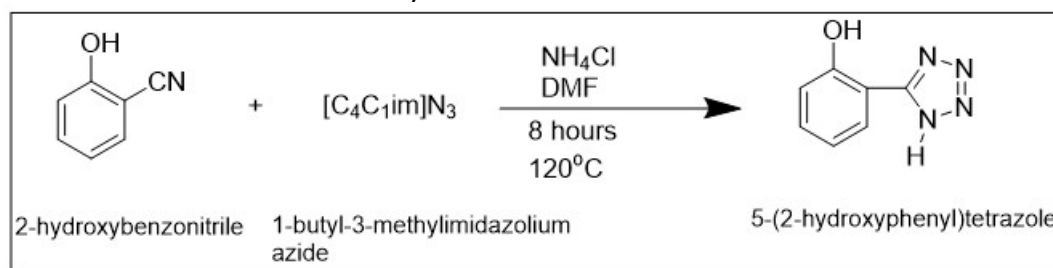
In the previous report, screening of various catalyst systems for the synthesis of different substituted tetrazoles were carried out. Along with that, determination of the cloud point temperature for the prepared ionic liquid, [P<sub>4444</sub>][2-OH-PhTet], for a few percentage compositions were measured using the Crystal 16. Additionally, a diagrammatic representation of the poster that was presented on the ILMAT-6 conference was shown.

#### Objective of this work

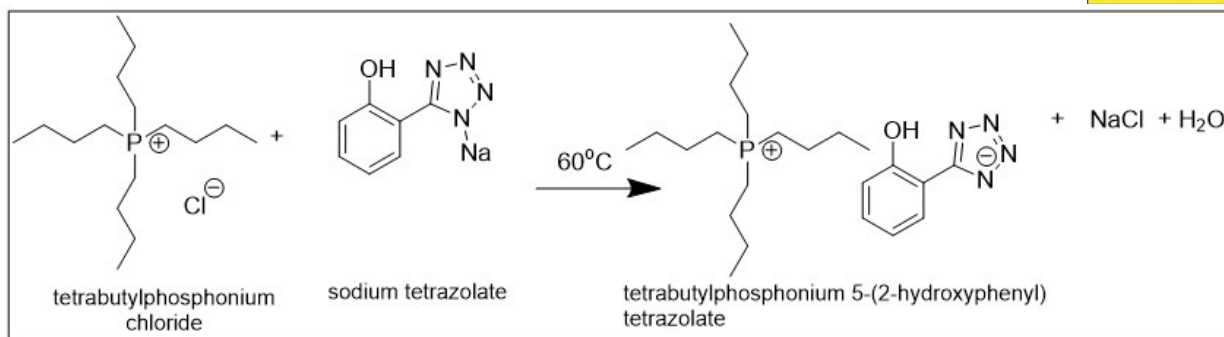
The prime objective of the work is to prepare and study various LCST ionic liquid systems bearing the tetrazole moiety and to compare their behaviour with those published previously by other groups. This will be done by designing the tetrazole with different functional groups with the result of synthesising the corresponding phosphonium-based ionic liquids. The ionic liquids that show the biphasic behaviour would be utilized as draw solutes in the forward osmosis process to desalinate sea water.

#### Progress to date

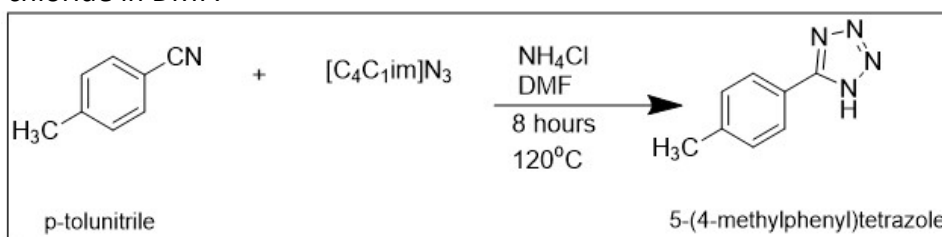
1. Synthesis of 5-(2-hydroxyphenyl)tetrazole from 1-butyl-3-methyl imidazolium azide, ammonium chloride in DMF with 96% yield.



2. Synthesis of tetrabutylphosphonium 5-(2-hydroxyphenyl)tetrazolate from tetrabutylphosphonium chloride and sodium tetrazolate.



3. Synthesis of 5-(4-methylphenyl)tetrazole from 1-butyl-3-methyl imidazolium azide, ammonium chloride in DMF.



#### Future work

1. To perform cloud point determination for the synthesised ionic liquid tetrabutylphosphonium 5-(2-hydroxyphenyl)tetrazolate for 10% to 90% composition (mass fraction) and salt concentrations.
2. To prepare the ionic liquid tetrabutylphosphonium 5-(4-methylphenyl)tetrazolate.
3. To obtain percentage of water content by Karl-Fischer titration of the two ionic liquids.
4. To compare the LCST of the two ionic liquids with that of the reported ones.
5. To find out methods of synthesising dicationic phosphonium based ionic liquids.



## QUILL Quarterly Report

November 2021 – January 2022

<b>Name:</b>	David McAreavey		
<b>Supervisor(s):</b>	Dr Stephen Glover, Dr Oana Istrate and Prof Peter Nockemann		
<b>Position:</b>	PhD Student		
<b>Start date:</b>	1 <sup>st</sup> October 2021	<b>Anticipated end date:</b>	31 <sup>st</sup> March 2025
<b>Funding body:</b>	Department for the Economy		

### Design and Development of an Effective and Interconnected Smart Fire Suppression System for Lithium-ion Batteries in Electric Vehicles

#### Background

As many countries around the world begin to implement their plans to ban the sale of new petrol and diesel vehicles in the coming decades, there is a clear shift occurring towards electrification of transportation. However, there are several challenges that should be addressed if mass adoption of these vehicles is to be successful. Chiefly among which are the needs to extend range and improve battery safety. Depending on the sources used it can be argued that EVs do have a good battery safety record and the number of electric vehicle fires that occur are relatively low. Tesla's 2020 vehicle safety report claims that one of their vehicles is almost ten times less likely to be involved in a vehicle fire than the average vehicle on the road in America per mile driven, based on data from the national Fire Protection Association and US department of transportation. Contrary to this, in London in 2019 based on data from the London Fire Brigade the incident rate when adjusted for the number of EVs and IC vehicles on the road is more than twice as high for EVs. Regardless of the exact frequency, due to the nature of these thermal events they can often initiate thermal runaway, meaning that it is extremely difficult to extinguish as well as having the potential to burn both hotter and longer than a typical IC vehicle fire. The primary concern is of course for the safety of the occupants of the vehicle and the potential danger to their health. Additionally, an EV has the potential to ignite in scenarios when nobody is around, usually an IC vehicle will ignite in use as this is when the highest temperatures are experienced. EVs on the other hand can ignite under circumstances such as when charging. This means that the thermal runaway process may go unnoticed for some time as well as likely being close to a home or garage causing significant property damage.

An additional concern surrounding the adoption of EVs is the level of media attention that EV fires receive. Despite being relatively infrequent especially due to the low total market share they hinder the adoption of these vehicles as well as causing the loss of resources that was originally carbon intensive to produce.

#### Objective of this work

The ultimate goal is to develop a fire suppression and thermal management system that can be realistically employed in a vehicle. This work may only achieve a step in this development, for such a suppression system. It is vital to consider that such a system must be compatible with thermal management systems as the implementation of a fire suppression system without an appropriate thermal management system essentially renders the vehicle useless. This means that a vehicle has the ability to keep the cells within its pack in the optimal temperature range, promoting longevity.



As well as having a sufficient suppression system that is able to prevent thermal runaway taking hold in the event of a fault or road traffic collision.

### **Progress to date**

The focus early on in this project was aimed mostly at early detection of thermal events including looking at a variety of sensors to develop a robust system. However due to the danger of thermal runaway of a cell it quickly became evident that the likelihood of being able to carry out real thermal runaway tests with the facilities available at Queen's was going to be very low. Additionally due to the unpredictable and highly complex nature of the mechanisms that underpin thermal runaway the use of a cell analogue would likely be a poor substitute.

As such the focus has since shifted towards the use of phase change materials in a hybrid thermal management system. Three potential gaps in the knowledge were identified for the initial review gateway that I undertook in January. These include the use of more than one phase change material, using two separate melting points. Secondly the simulation of a full EV thermal runaway and thermal management system. Most literature to date is quite narrowly focussed on either thermal management or runaway prevention at a relatively low level, typically not looking at the wider perspective of implementation into an EV. This could include looking at the radiator, pump, fans ect used in a hybrid system alongside the weight and volume penalty that would be incurred from using PCM in a battery pack. Finally, the development of a system that uses PCM to remove part of the heat form a vehicle while also providing improved access for first responders was also proposed. The direction of the project will be defined by the completion of initial modelling to determine the feasibility of these three avenues.

Since the completion of initial review the focus has been on developing the early stage building blocks of a Matlab model that will be the basis of the feasibility study. Initially the modelling will be quite basic with the full complexity of the model being built in over time. At this stage a steady state PCM model has been created and a steady state liquid cooling model. The next step will be the combination of these two models before adding in additional elements that will more accurately represent reality.

### **Conclusions and future work**

The results from the initial modelling will be the next major development as they will inform what is a feasible gap in the knowledge to follow for this project. As such that is the focus of the future work. This will culminate in differentiation that takes place in June/July for this project.

## QUILL Quarterly Report

November 2021 – January 2022

<b>Name:</b>	Sam McCalmont		
<b>Supervisor(s):</b>	Dr Leila Moura, Prof John Holbrey and Prof Margarida Costa Gomes		
<b>Position:</b>	PhD		
<b>Start date:</b>	Jan 2020	<b>Anticipated end date:</b>	2023
<b>Funding body:</b>	EPSRC Doctoral Training Partnership		

### Chemisorbent materials for olefin and paraffin separation

#### Background

Separation of light olefins from their paraffin counterparts have been described as one of the seven chemical separations to change the world.<sup>1</sup> Global annual production of light olefins exceeds 200 million tons, about 30 kg for each person on the planet. The current method for their separation is cryogenic distillation, one of the most energy-intensive processes in the industry. Alternative methods can focus on the olefin being selectively captured either through a physical interaction (physisorption) or chemical reaction (chemisorption).

One class of alternative sorbents are ionic liquids (ILs). However, so far, IL physisorbents have not demonstrated sufficient efficiency in either selectivity or capacity to compete with current technologies.<sup>2</sup> Complexation of ethylene through its double bond with silver and copper ions has been used for chemical separation of olefins and paraffins. However, other components of raw gas feeds, such as acetylene, can react with the silver and become explosive. This has prevented the uptake of these materials into large scale processes.

#### Objective of this work

To develop and test new chemisorbent materials for the separation of light olefins and paraffins; to achieve high capacity combined with selectivity for the selected materials. To investigate, and rationalise, selectivity and capacities of chemisorbents based on measurement of gas solubility and partitioning from model industrial gas stream compositions and conditions.

#### Progress to date

Over the last three months, investigation of two groups of ionic liquids has been undertaken. The two groups are: (i) cyanopyridinium based ionic liquids and (ii) ionic liquids incorporating dissolved metal species (not silver and copper). Both groups of ionic liquid systems are being examined for ethylene/ethane separation via the gas solubility system (GSS) and screening method.

Cyanopyridinium ionic liquids synthesised, and previously reported (butyl-4-cyanopyridinium bis(trifluoromethylsulfonyl)imide  $[\text{C}_4^4\text{CNPY}][\text{NTf}_2]$ ) and butyl-3-cyanopyridinium bis(trifluoromethylsulfonyl)imide  $[\text{C}_4^3\text{CNPY}][\text{NTf}_2]$ ) (figure 1) are currently being tested via the screening method and the GSS. The screening method allows for both pure ethylene tests, pure ethane tests and also for a mixture of ethylene/ethane to more mimic industrial conditions. The presence of the electron-withdrawing nitrile group may have two potential roles in modifying gas selectivity; either providing a  $\pi$ -electron-rich site for olefin association (matching enhancement in solubility of ethylene in terminal-nitrile chain substituted ionic liquids) or through induction of olefin  $\pi$ -electron association with the electron-deficient aromatic cation of the ionic liquid (as reported

from cyanopyridinium-polyaromatic hydrocarbon mixtures). To further explore and rationalise potential interaction mechanisms, additional ionic liquids incorporating di-cyanopyridinium cations have been designed and are under investigation.

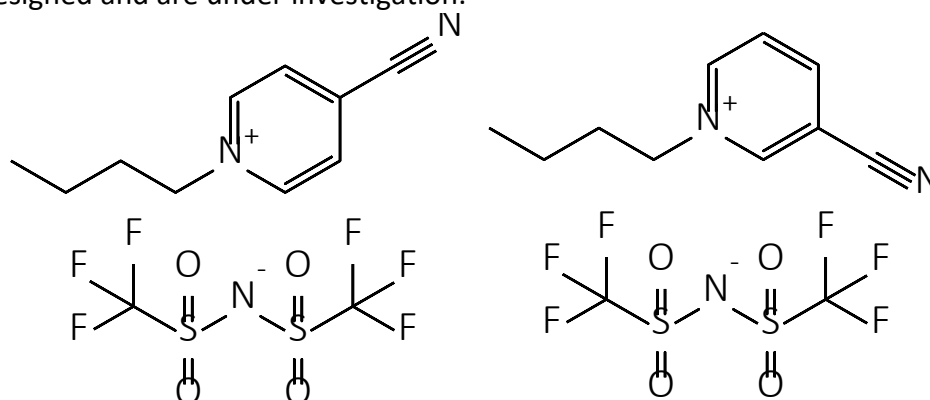


**Figure 1** - Butyl-4-cyanopyridinium bis(trifluoromethylsulfonyl)imide (left) and butyl-3-cyanopyridinium bis(trifluoromethylsulfonyl)imide (right).

Preliminary results from the screening method are shown below for  $[\text{C}_4^4\text{CNPy}][\text{NTf}_2]$  (figure 2) and  $[\text{C}_4^3\text{CNPy}][\text{NTf}_2]$  (figure 3). Measurement is still ongoing, but these results show a greater affinity for ethylene compared to ethane as anticipated. Gas uptake is similar in magnitude to that determined with the benchmark,  $[\text{bmim}][\text{NTf}_2]$ .

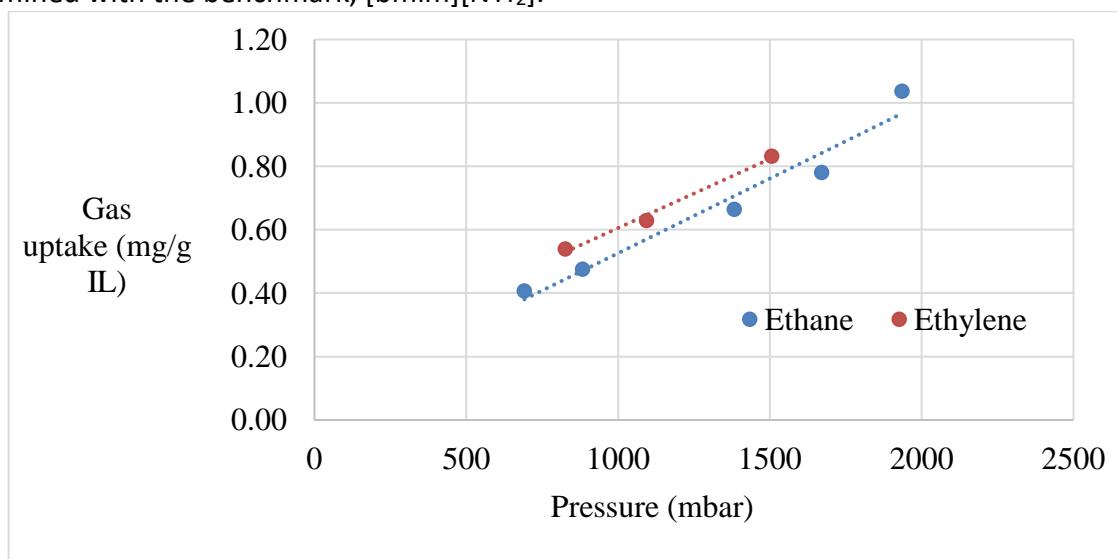


**Figure 2** - Initial uptakes of ethylene and ethane for  $[\text{C}_4^4\text{CNPy}][\text{NTf}_2]$

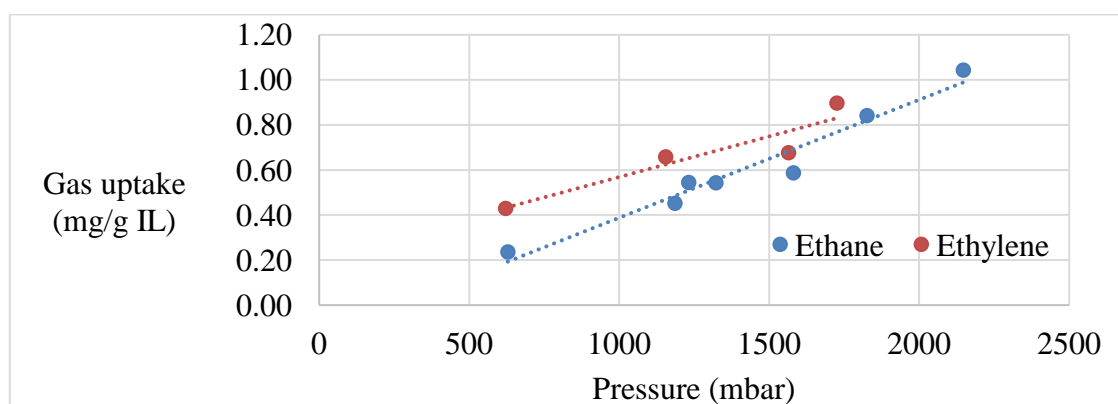


**Figure 3** - Initial uptakes of ethylene and ethane for  $[\text{C}_4^3\text{CNPy}][\text{NTf}_2]$





The second group of ionic liquids to be tested involve introducing different metal species into [bmim]Cl (testing the complexes formed) and [bmim][NTf<sub>2</sub>] to determine whether the enhanced selectivity to ethylene that is well known with dissolved silver and copper species can be replicated using other alternative metal species. Screening and assessment of a range of metals in these two base ionic liquids, with solubility tests (to determine metal salt solubility and miscibility in the ILs) and then measurement of gas solubility of ethylene, ethane, and ethylene/ethane mixtures as a function of partial pressure has been started.

### Conclusions and future work

In the coming weeks, the plan is to move forward to test the materials created with a gas mixture to closer study the separation potential between ethylene and ethane. This will involve creating new cyanopyridinium ionic liquids and testing the metals further.

### References

1. D. S. Sholl and R. P. Lively, *Nature*, 2016, 532, 435–437.
2. L. Moura, C. C. Santini and M. F. Costa Gomes, *Oil Gas Sci. Technol. – Rev. d'IFP Energies Nouv.*, 2016, **71**, 23.
3. C. Hardacre, J. D. Holbrey, C. L. Mullan, M. Nieuwenhuyzen, T. G. A. Youngs, D. T. Bowron and S. J. Teat, *Phys. Chem. Chem. Phys.*, 2010, **12**, 1842–1853.





### Progress to date

The oligomerisation of 1-decene has been carried out using a liquid coordination complex,  $\text{Ur-AlCl}_3$   $\chi = 0.60$ .

Reaction conditions, 100 °C, 60 mins, 1-decene (60 ml)  $\text{Ur-AlCl}_3$   $\chi = 0.60$ .

Reaction code	Catalyst amount (g)	Product (g)	Yield
emc-03	0.34	21.47	50.97
emc-04	0.34	17.323	40.27
emc-05	0.34	22.32	51.11
emc-06	0.68	31.583	73.22
emc-07	0.68	29.07	68.01

### Conclusions and future work

The yield and the repeatability have been obtained and the procedure optimised. This will allow comparison when the naphta fraction is used in the oligomerisation. The oligomerisation of 1-decene using borenium ionic liquid and using the naphta fraction are the next steps.

## QUILL Quarterly Report

November 2021 – January 2022

<b>Name:</b>	Anne McGrogan		
<b>Supervisor(s):</b>	Prof Gosia Swadzba-Kwasny		
<b>Position:</b>	PhD		
<b>Start date:</b>	01/10/2019	<b>Anticipated end date:</b>	31/03/2023
<b>Funding body:</b>	EPSRC		

### Boron Lewis acids: structure and applications

#### Background

Many boron compounds are Lewis acidic, either due to the presence of a free  $p$  orbital in species with  $sp^2$ -hybridised boron, or due to labile ligands attached to  $sp^3$ -hybridised boron that can be readily replaced by a nucleophile.<sup>1</sup> Quantifying Lewis acidity of these various boron compounds is very challenging, which to a certain extent hinders understanding of their reactivity.

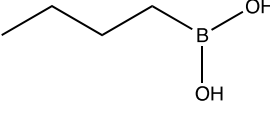
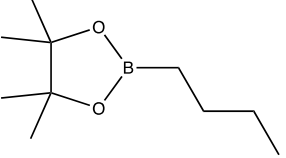
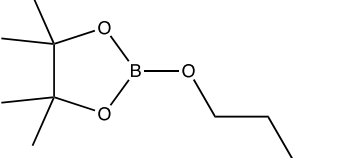
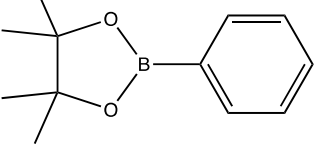
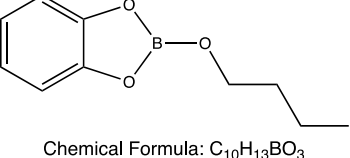
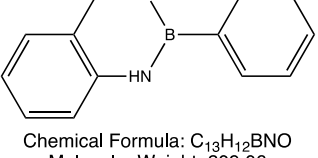
Our group has a long-standing interest in Lewis acidic ionic liquids, which has led us to the development of ionic liquids with tricoordinate, Lewis superacidic borenium cations.<sup>1</sup> Their acidity was quantified using the Gutmann acceptor number,<sup>2</sup> the most common method for probing Lewis acidity of ionic liquids. However, as a method based on a  $^{31}\text{P}$  NMR spectroscopic probe (triethylphosphine oxide), Gutmann's approach is necessarily dependent on hard-soft acid-base (HSAB) explanations. Lewis acidity is measured against a single base and it is not sufficient to compare compounds of widely differing Lewis acidities. It does not give insight into different factors influencing Lewis acidity: hardness/softness of acid/base in a Lewis adduct, electronic environment of boron, energy required to alter geometry around the boron centre upon the adduct formation.

In this work we have set out to study directly the electronic environment of boron using liquid jet X-ray photoelectron spectroscopy (XPS). Boron 1s X-ray spectroscopy is not commonly measured due to extensive experimental challenges, especially in the liquid phase. This technique does not require the probe and is very much complementary to the Gutmann's method. By understanding how the electronic structure relates to chemical reactivity and probe-based Lewis acidity measurements, we aim to elucidate different factors that influence Lewis acidity, and understand how each impacts the catalytic performance of boron Lewis acids.

#### Progress to date

The experiments were performed at the BESSY II synchrotron, Berlin, using a combination of liquid-jet sample delivery with XPS, resonant XPS and X-ray absorption spectroscopy (XAS). Six boron compounds were studied (Table 1).

**Table 1** - Boron compounds studied by XPS at the at the BESSY II synchrotron, Berlin.

Sample	Code Name	Lab book name	Chemical formula/Structure
1	Butylboronic acid	Butylboronic acid	 Chemical Formula: $C_4H_{11}BO_2$ Molecular Weight: 101.94
2	B(pin)(Bu)	Butyl boronic acid pinacol ester	 Chemical Formula: $C_{10}H_{21}BO_2$ Molecular Weight: 184.09
3	B(pin)(OBu)	Butyl borate pinacol ester	 Chemical Formula: $C_{10}H_{21}BO_3$ Molecular Weight: 200.09
4	PhB(pin)	Phenylboronic acid pinacol ester	 Chemical Formula: $C_{12}H_{17}BO_2$ Molecular Weight: 204.08
5	B(cat)(OBu)	Butyl borate catechol ester	 Chemical Formula: $C_{10}H_{13}BO_3$ Molecular Weight: 192.02
6	PhB(C7H9NO)	Phenyl boronic acid 2-amino benzyl alcohol ester	 Chemical Formula: $C_{13}H_{12}BNO$ Molecular Weight: 209.06

Preliminary results validate the new approach of measuring boron 1s X-ray spectroscopy to provide insight into Lewis acidity of tricoordinate compounds of boron.

### Conclusions and future work

I am currently learning how to use IGOR and CasaXPS software which I will use for the analysis of the XPS data.

I am also currently analysing data collected by neutron scattering looking at the structure of derived protic ionic liquids based on sulfuric acid using DISSOLVE software.

## QUILL Quarterly Report

November 2021 – January 2022

<b>Name:</b>	Shannon McLaughlin		
<b>Supervisor(s):</b>	Prof Gosia Swadźba-Kwaśny		
<b>Position:</b>	PhD Student (2 <sup>nd</sup> year)		
<b>Start date:</b>	October 2020	<b>Anticipated end date:</b>	July 2024
<b>Funding body:</b>	Department for the Economy		

### Thinking inside the (glove)box: Lewis Superacidic Ionic Liquids Based on Main Group Cations

The chemistry of Lewis acidic main group cations is of increasing importance, as metal-free catalysis gains interest of the scientific community. One of the longest-standing challenges in main group synthetic chemistry has been the preparation of tricoordinate, tetravalent silicon cations in the condensed phase. Silylium ions are extremely Lewis acidic and have a high electrophilicity, oxophilicity and fluorophilicity, affording unique transformations that cannot be performed by traditional metal catalysts. Recently, synthetic methods to generate stable silylium cations have become more accessible and more effective.

Silylium ions can be categorised as either stabilised or ‘free’. As they are highly reactive, silicon cations are commonly found as species which are stabilised, whereas ‘free’ silicon cations are extremely rare. The first ever ‘free’ silylium cation to be isolated was the trimesitylsilylium cation ((Mes)<sub>3</sub>Si<sup>+</sup>) (**1**).<sup>1</sup> The tridurylsilylium cation ((duryl)Si<sup>+</sup>) (**2**)<sup>2</sup> was later isolated along with the related species (C<sub>6</sub>Me<sub>5</sub>)<sub>3</sub>Si<sup>+</sup> (**3**).<sup>3</sup> Till date these three compounds are the only examples of ‘free’ species whose structures have been confirmed by X-ray crystallography.

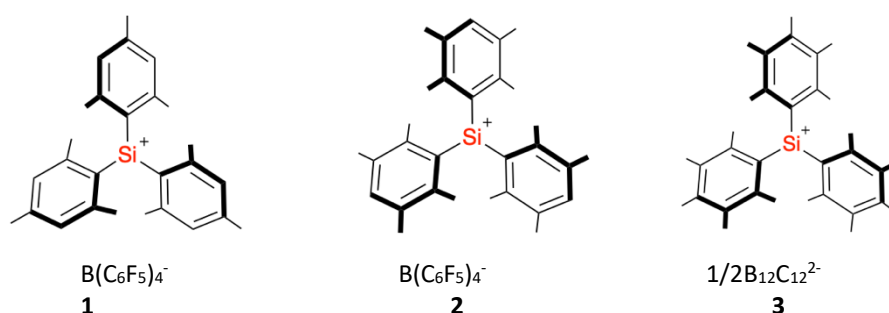


**Figure 1** - Structure of (Mes)<sub>3</sub>Si<sup>+</sup>, (duryl)Si<sup>+</sup> and (C<sub>6</sub>Me<sub>5</sub>)<sub>3</sub>Si<sup>+</sup>.

There is a particular interest into cationic silicon compounds in this project and the first goal is to synthesise the ‘free’ trimesitylsilylium cation first isolated by Lambert *et al.*<sup>1</sup> The synthesis of trimesitylsilane, chlorotrimesitylsilane, and allyltrimesitylsilane will follow methods described by Lappert *et al.*,<sup>4</sup> Zigler *et al.*<sup>5</sup> and Lambert and Zhao,<sup>1</sup> respectively. The allyltrimesitylsilane will be used to synthesise the ‘free’ trimesitylsilylium cation following the method described by Lambert *et al.*<sup>1</sup> Silylium ions are usually quite a reactive species but the bulky mesityl groups in compound **1** help to shield the silicon centre from attack by large nucleophiles. These steric interactions also

prevent the silylium ion reacting with the solvent and the product alkene making it much more stable.

This work reports on the first-ever attempt to prepare and characterise silylium ionic liquids, where the cations shown in Figure 1 are combined with non-coordinating anions, such as  $[B(C_6F_5)]^-$ ,  $[NTf_2]^-$  and  $[eFAP]^-$ .

### Synthesis of trimesitylsilane:

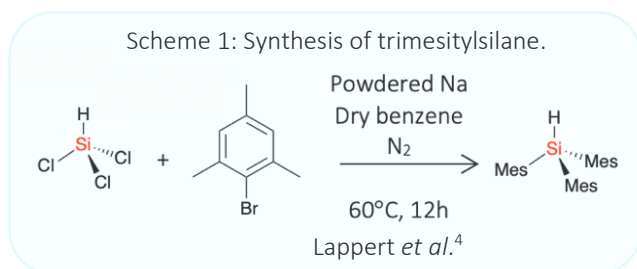


**Figure 2** - i) White crystals of trimesitylsilane (first batch).  
ii) White crystals of trimesitylsilane and yellow liquid which contains impurities (second batch).

Trimesitylsilylium was synthesised following the method described by Lappert *et al.*<sup>4</sup> In a previous batch, 3.02 g of trimesitylsilane was synthesised giving a percentage yield of 38.8% (white crystals shown in Figure 2). A second batch of trimesitylsilylium was synthesised to increase the yield.

$^1H$ ,  $^{13}C$  and  $^{29}Si$  NMR spectra for trimesitylsilane were recorded,  $^1H$  and  $^{29}Si$  NMRs are shown in Figure 3 and Figure 4, respectively. Peaks observed matched exactly to literature values in all NMR spectra.

$^1H$  NMR (600 MHz,  $CDCl_3$ )  $\delta$ : 2.12 (s, 18H), 2.26 (s, 9H), 5.75 (s, 1H), 6.78 (s, 6H).

$^{13}C$  NMR (600 MHz,  $CDCl_3$ )  $\delta$ : 21.14 ppm (p- $CH_3$ ), 23.42 ppm (o- $CH_3$ ), 128.93 ppm ( $C_{meta}$ ), 131.23 ppm ( $C_{para}$ ), 138.96 ppm, ( $C_{ortho}$ ), 144.80 ppm ( $C_{ipso}$ ).

$^{29}Si$  NMR (600 MHz,  $CDCl_3$ )  $\delta$ : -44.34 ppm.

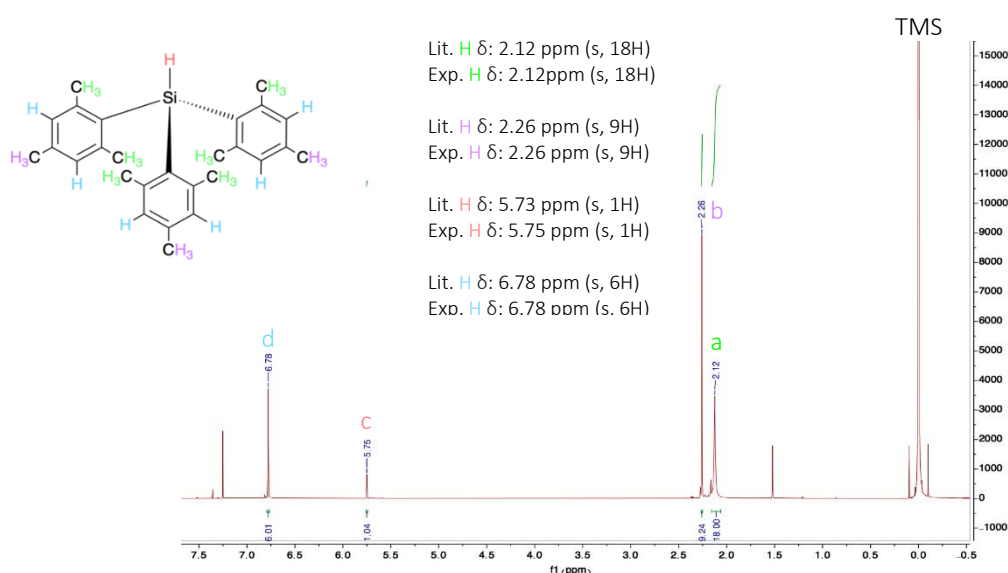


**Figure 3** -  $^1H$  NMR spectrum of trimesitylsilane in  $CDCl_3$ .

TMS

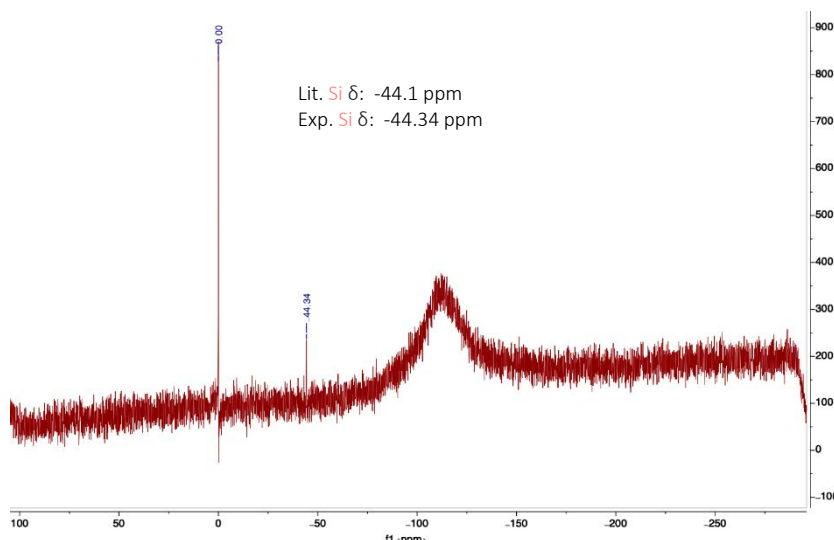
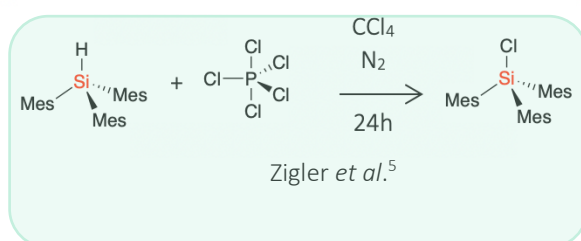


**Figure 4** -  $^{29}\text{Si}$  NMR spectrum of trimesitylsilane in  $\text{CDCl}_3$ .

Synthesis of chlorotrimesitylsilane:

**Scheme 2** - Synthesis of chlorotrimesitylsilane.



Chlorotrimesitylsilylium was synthesised following methods described by Zigler *et al.*<sup>5</sup> A second batch of chlorotrimesitylsilylium was synthesised to increase the yield.  $^1\text{H}$ ,  $^{13}\text{C}$  and  $^{29}\text{Si}$  NMR spectra of each sample were recorded to confirm purity. Both batches of chlorotrimesitylsilane were combined before moving onto the synthesis of allyltrimesitylsilane.

$^1\text{H}$  NMR is shown in Figure 5. Excess peaks were present due to impurities and solvents. Methanol appears as a singlet at 3.49 ppm and hexane appears as a triplet at 0.88 ppm and a multiplet at approximately 1.26 ppm. There is also a small amount of starting reagent remaining at 5.75 ppm. The reaction mixture will be refluxed again until no starting reagent can be detected and then dried thoroughly on the Schlenk line to remove the solvent impurities.

$^1\text{H}$  NMR (600 MHz,  $\text{CDCl}_3$ )  $\delta$ : 1.96 – 2.46 (br, 18H), 2.24 (s, 9H), 6.72 – 6.90 (br, 6H).

$^{13}\text{C}$  NMR (600 MHz,  $\text{CDCl}_3$ )  $\delta$ : 20.02 ppm (p- $\text{CH}_3$ ), 23.97 ppm (o- $\text{CH}_3$ ), 127.88 ppm ( $\text{C}_{\text{meta}}$ ), 131.92 ppm ( $\text{C}_{\text{para}}$ ), 138.66 ppm ( $\text{C}_{\text{ortho}}$ ), 143.75 ppm ( $\text{C}_{\text{ipso}}$ ).



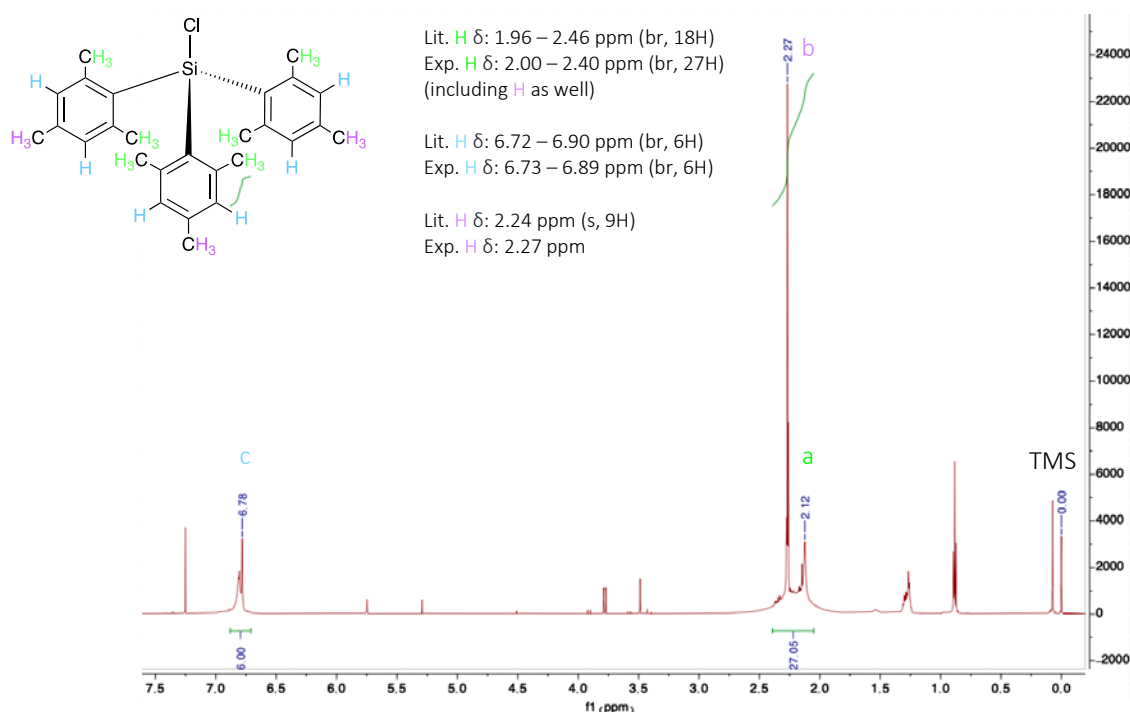


**Figure 5** -  $^1\text{H}$  NMR spectrum of chlorotrimesitylsilane in  $\text{CDCl}_3$ .

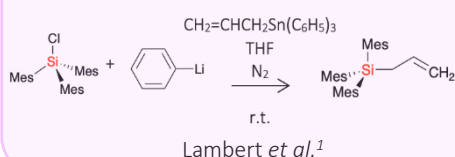
## Future Work

Synthesis of allyltrimesitylsilane and a 'free' trimesitylsilylium cation:

Future work will involve completing the final two steps of the proposed synthesis of the 'free' trimesitylsilylium cation.

Allyltrimesitylsilane and trimesitylsilylium tetrakis(pentafluorophenyl)borate (compound **1**) will be synthesised following methods described by Lambert *et al.*<sup>1</sup> and Lambert and Zhao<sup>6</sup> respectively. An allyl leaving group method is used to generate the free silicon cation and the corresponding alkene. The driving force for this reaction is provided by the relief of steric strain around the original tetracoordinate silicon centre. These salts are difficult to crystallise properly and instead they tend to form oils or liquid clathrates. Therefore, there is a potential to use these materials for unique applications such as ionic liquids. They will also be employed as a potential catalyst for both racemic and enantioselective Diels-Alder reactions, activation of strong carbon-fluorine bonds and the Friedel-Crafts silylation of heteroaromatic compounds. After compound **1** has been successfully synthesised, it will be combined with commonly used anions such as  $[\text{B}(\text{C}_6\text{F}_5)_4]^-$ ,  $[\text{NTf}_2]^-$ ,  $[\text{FSI}]^-$  and  $[\text{eFAP}]^-$  to conduct characteristic studies of the cation.

**Scheme 3: Synthesis of allyltrimesitylsilane.**



**Scheme 4: Synthesis of a 'free' trimesitylsilylium cation.**



The next aim would be to combine the trimesitylsilylium cation with borate anions or cyanoborate anions (Figure 6) in hope of generating new Lewis superacidic ionic liquids. Applications of these newly developed ionic liquids will then be investigated for potential use as solvents and catalysts.

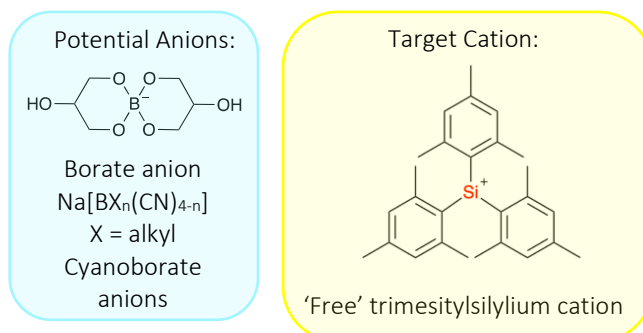


**Figure 6** - Structure of the target trimesitylsilylium cation and potential borate anions or cyanoborate anions.

## References

1. K. C. Kim, C. A. Reed, D. W. Elliott, L. J. Mueller, F. Tham, L. Lin and J. B. Lambert, *Science.*, 2002, **297**, 825–827.
2. J. B. Lambert and L. Lin, 2001, *J. Org. Chem.*, 66, 8537–8539.
3. A. Schäfer, M. Reißmann, S. Jung, A. Schäfer, W. Saak, E. Brendler and T. Müller, 2013, *Organometallics*, 32, 4713-4722.
4. M. Gynane, M. Lappert, P. Riley, P. Rivière and M. Rivière-Baudet, *Journal of Organometallic Chemistry*, 1980, **202**, 5-12.
5. S. Zigler, L. Johnson and R. West, *Journal of Organometallic Chemistry*, 1988, **341**, 187-198.
6. J. Lambert, C. Stern, Y. Zhao, W. Tse, C. Shawl, K. Lentz and L. Kania, *Journal of Organometallic Chemistry*, 1998, **568**, 21-31.



## QUILL Quarterly Report

November 2021 – January 2022

<b>Name:</b>	Hugh O'Connor		
<b>Supervisor(s):</b>	Prof Peter Nockemann, Dr Stephen Glover and Dr Josh Bailey		
<b>Position:</b>	PhD Student		
<b>Start date:</b>	October 2019	<b>Anticipated end date:</b>	June 2023
<b>Funding body:</b>	EPSRC		

### Redox Flow Battery Materials for Energy Storage

#### Background

As fossil fuel supplies dwindle and the climate change problem escalates, the need to harness renewable energy resources increases. However, these energy sources are intermittent and unpredictable, making them difficult to be used in a safe and stable power grid. For this reason, it is important that new energy storage technologies are developed which can shift energy from off-peak demand times to peak demand times. One of the most promising emerging technologies is the redox flow battery (RFB).

In RFBs, redox couples are dissolved in electrolyte solutions and stored in separate reservoir tanks. During charge and discharge these electrolytes are pumped from reservoir tanks into half cells where they react in an electrode, either consuming or generating electrons.

This working principle gives rise to a number of key advantages over other conventional battery technologies. In flow batteries, power and energy is decoupled; power is controlled by the stack effectiveness whilst energy is stored in the electrolyte reservoir tanks. This makes RFBs highly customisable, allowing them to be tailored to meet the demands of various power grids. They also have a long working life; with the electrolytes stored in separate tanks, the electrodes don't undergo complex redox reactions and experience less structural changes and strain than those found in conventional batteries. One drawback of RFBs however is their low energy density and high costs when compared to other energy storage technologies.

Improving the energy density, energy storage efficiency and sustainability could make RFBs an even more promising candidate for large scale energy storage applications. Innovative and more efficient manufacturing techniques could also potentially provide a solution in reducing inevitable costs that will occur when implementing a new energy storage technology.

One method of improving the performance of RFBs is designing better performing flow fields, manifolds and cell stack topologies resulting in a better performing cell stack

#### Objective of this work

To investigate the effect of modified cell topology and stack architecture on the power density of redox flow batteries, identifying key performance influencers and improving economic viability.



### **Progress to date**

Extensive work has been carried out into the investigation of novel cell and manifold topologies to improve cell performance. Fused Deposition Modelling (FDM) 3D-printing has been identified as a powerful tool to produce lab scale RFB test cells at an extremely low cost. Print parameters have been refined to best suit flow cell manufacture, resulting in robust leak proof test cells. Furthermore, this rapid prototyping approach coupled with CFD/ electrochemical modelling appears an effective approach to iteratively refine flow cell design. These findings have been written up and published in a paper for the RSC journal Sustainable energy and fuels. Following on from this work, these cells have been scaled up in order to allow for a wider range of cell designs to be evaluated. Economic viability of FDM in order to manufacture larger scale flow cells is being carried out alongside the design of stackable test cells. Work is also ongoing into the improvement of FDM 3D-printed polypropylene in for use in wider flow electrochemistry applications.

### **Conclusions and future work**

FDM 3D-printing has proven an invaluable tool in producing fully customisable low-cost test cells in order to allow for the development of new cell topologies and materials. The platform developed is being utilised and expanded to further research into improved flow cell design.

## QUILL Quarterly Report

November 2021 – January 2022

<b>Name:</b>	Liam O'Connor		
<b>Supervisor(s):</b>	Dr Oana Istrate and Prof B Chen		
<b>Position:</b>	PhD student		
<b>Start date:</b>	01 <sup>st</sup> Oct 2020	<b>Anticipated end date:</b>	29 <sup>th</sup> Sept 2023
<b>Funding body:</b>	Department for the Economy		

### 3D-printed polymer graphene nanocomposites for biosensor applications

#### Background

A polymer strain sensor works on the principle that the electrical conductivity is proportional to the mechanical strain applied. Thus far, literature has focused on the prosthetic using feedback from pressure sensors in the fingertip to give feedback to the user. One of the limitations of using this pressure sensor is that it can only distinguish objects within the surface area of the sensors, which is 15 mm<sup>2</sup>. An important feature of the material used to manufacture a prosthetic arm is that it needs to be 3D printable. 3D printing allows for freedom of form, thus enabling for the prosthetic arms to be customised. The materials investigated in this study are thermoplastic polyurethane (TPU) because of its strong hysteresis response to mechanical strain, nylon-11 (PA11) because of its piezoelectric properties, and graphene nanoplatelets (GNPs) due to their ability to increase the electrical conductivity of other piezoelectric polymers, such as polyvinylidene fluoride (PVDF).

#### The objective of this work

The objective of the work is to develop a strain-dependent electrically conducting material that could be used as a strain sensor and can be 3D printed through fused deposition modelling. This will be done by determining the optimal graphene for the manufacturing of TPU/GNP filaments, determining the optimal graphene loading for the manufacturing of PA11/GNP filaments, determining the optimal graphene loading for the manufacturing of TPU/PA11/GNP filaments, and determining the optimal manufacturing layering structure for TPU/PA11/GNP filaments.

#### Progress to date

Characterisation of the TPU nanocomposite has shown that the GNPs tend to gravitate towards hard domains of the polymer matrix, which mainly consist of rigid diisocyanate and chain extender moieties. The Young's modulus of the TPU nanocomposite increased by 21 %, compared to the neat TPU, at a loading of 1.5 wt.% with no detrimental effect to the elasticity of the nanocomposite.

Characterisation of the PA11 nanocomposite has shown that the GNPs are attracted to the hydrogen bonds formed between the polymer chains, which prevents the polymer chains from rotating and forming  $\delta$  crystals. An electrical percolation threshold was found at 8.1 wt. % and a rheological percolation threshold was found at 9.3 wt. %

#### Conclusions and future work

The next stage is to investigate the dispersion within the PA11 nanocomposite and decide on a weight percent's of GNP to use in the TPU/PA11 nanocomposite.

## QUILL Quarterly Report

November 2021 – January 2022

<b>Name:</b>	Scott Place		
<b>Supervisor(s):</b>	Dr Paul Kavanagh (Primary) and Dr Mark Muldoon (Secondary)		
<b>Position:</b>	PhD Student		
<b>Start date:</b>	Oct 2019	<b>Anticipated end date:</b>	Jul 2023
<b>Funding body:</b>	EPSRC		

## Molecular Electrocatalysts for Energy and Electrosynthetic Applications

### Background

This project focuses on the nitroxide radical molecule TEMPO and its derivatives, their electrokinetic properties, and their applications in energy storage, energy generation, and electrosynthetic applications. TEMPO-like molecules are able to be electrochemically oxidised at an electrode surface to an active oxoammonium form, which can then react with substrates in a chemical redox reaction, which regenerates them to their nitroxide (or hydroxide, when protons are present) form. These reactions follow the well-established EC' (electrochemical-chemical) two-step reaction profile, studied extensively by Savéant and co-workers and Dempsey and co-workers, among others.

Electrolysis for organic synthesis is gaining popularity in the literature as a low-waste and simple procedure for converting a number of substrates to their corresponding products. TEMPO and its derivatives are an example of chemicals that can be used as electrocatalysts for oxidation reactions, where direct electrochemical oxidation of the substrate may be too energy-intensive.

### Objective of this work

In this part of the study, we aim to use the TEMPO-mediated oxidation of benzyl alcohol as a benchmarking case study, where develop an electrochemical method of catalyst benchmarking in a synthetic context. Many organic chemists have had little exposure to electrochemistry in their careers, and may find some of the calculations, rate constants, and other electrochemical parameters unclear. We aim to develop a straightforward method of electrochemical catalyst benchmarking (using such techniques as cyclic voltammetry and chronoamperometry) and elucidate the relationship between calculated electrochemical parameters and their usefulness in organic synthesis. Similar efforts have been made in the context of catalyst benchmarking for hydrogen generation for the energy industry, but none in the context of organic synthesis.

### Progress to date

Over the last three months, work has been underway on developing a method that will allow the use of the Savéant method for electrocatalyst kinetic analysis. Conditions such as pseudo-first order conditions and scan rate independence must be established to extract comparable rate constants using Savéant's models. Additionally, electrolysis experiments are being optimised for comparisons of conversion and yield when using a number of different TEMPO derivatives. Monitoring the reaction has been challenging, as efforts to optimise HPLC analysis proved unfruitful. We are now using NMR with an internal standard, which appears promising. A full run of standardised model electrolysis experiments for comparison of the different electrocatalysts will soon be underway, alongside significant teaching responsibilities within the university.



### **Conclusions and future work**

The last three months have been strongly focused on method optimisation for the electrolysis study. Over the coming few months, work will be underway to determine conversion and yield percentages for a number of TEMPO derivatives' oxidation of benzyl alcohol. This will then be related to calculated electrochemical parameters, and conclusions drawn. We will identify strengths and weaknesses of electrochemical characterisation of catalysts using cyclic voltammetry and chronoamperometry and make a number of suggestions for future benchmarking studies.

## QUILL Quarterly Report

November 2021 – January 2022

<b>Name:</b>	Junzhe Quan		
<b>Supervisor(s):</b>	Prof John Holbrey and Dr Leila Moura		
<b>Position:</b>	PhD		
<b>Start date:</b>	01/10/2019	<b>Anticipated end date:</b>	01/10/2023
<b>Funding body:</b>	Self funding		

### Use ionic liquids that exhibit LCST (lower critical solution temperature) behaviour as draw fluids for water treatment, desalination and separation

#### Background

New Ionic liquid materials have been recently developed that exhibit lower critical solubility temperature (LCST) behaviour with water, that is, they are miscible at a low temperature and split into two aqueous phases on heating beyond a critical temperature. Such materials have the potential to be used as draw fluids for forward osmosis (FO) water desalination using low grade energy to address the global challenge to provide clean, accessible drinking water to all the world's populations. In this research programme, new ionic liquids will be investigated as advanced fluids for forward osmosis water treatment. This offers opportunities to advance less energy intensive alternative to conventional reverse osmosis as a solution to the global challenge of providing potable water in regions of low availability.

#### Objective of this work

My research program in the use of ionic liquids as potential draw fluids for FO water treatment includes:

Preparation of appropriate model ionic liquids.

Characterisation of aqueous/ionic liquid phase behaviour as a function of aqueous component salinity, pH, temperature and to draw structure-performance relationships with the ionic liquid cation/anion components.

Develop a FO membrane cell to test and evaluate draw fluid characteristics and parameters of selected systems.

Optimize ionic liquid to use as draw fluid, developing a proof-of-concept ionic liquid-based FO desalination demonstrator for benchmarking.

Examine the applicability of these draw fluids to water-processing of a range of feeds and product streams (desalination, waste concentration, biomass dewatering).

Measure the energy consumption and compare with typical method of water treatment.

#### Progress to date

Experimental: Three ionic liquids that have been reported to exhibit LCST behaviour in water (tetrabutylphosphonium 5-phenyltetrazolate, tetrabutylphosphonium salicylate and tetrabutylphosphonium p-toluenesulfonate) have been synthesised and fully characterised. These ionic liquids contain the same cation and have the three aromatic anion motifs that are of interest for comparative understanding of performance. The impact of salt (NaCl) content on the LCST of



aqueous/IL mixtures with the three ILs has been examined by screening the cloud point temperatures by turbidity measurement using the Avantium Crystal16 at 50% mass fraction IL:water with saline (sodium chloride)solutions.

Results: LLE phase diagrams are reported in different salinity.

Salt concentration(g/L)	0	20	30	40	50	60	80	100	120
Cloud points temperature (°C) of 50% mass fraction Ph-tet/salt solution mixtures	38.5	32.2	30.5	29.1	26.3	24.4	19	14.8	10.9

**Table 1** - Cloud points of [P<sub>4444</sub>][Ph-tet]

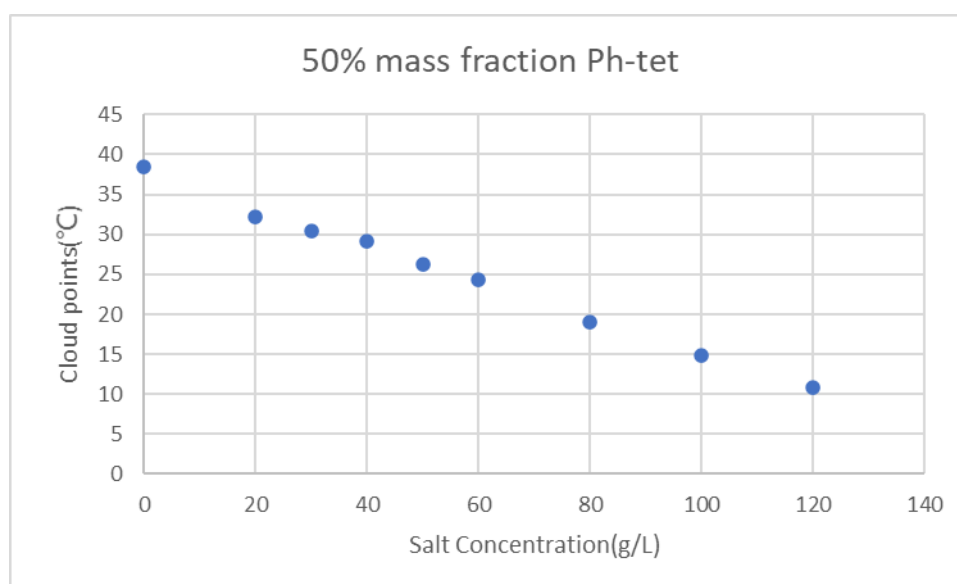


**Figure 1** - Cloud points of [P<sub>4444</sub>][Ph-tet] under different salt concentration in 50% mass fraction IL concentration

Salt concentration(g/L)	0	20	30	40	50	60	80
Cloud points temperature (°C) of 50% mass fraction Sal/salt solution mixtures	31.4	26.3	23.7	22.9	21.1	18.6	13.9

**Table 2** - Cloud points of [P<sub>4444</sub>][Sal]

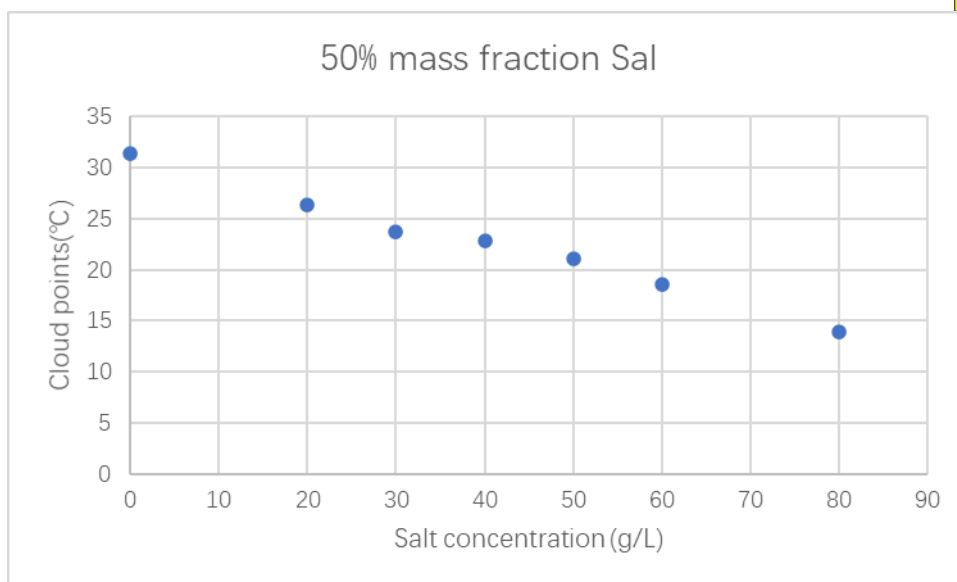


**Figure 2** - Cloud points of  $[P_{4444}][Sal]$  under different salt concentration in 50% mass fraction IL concentration

In figure1 and figure 2, it shows a strong correlative behaviour between the relative salt concentration(NaCl) in solution and the change in cloud points.

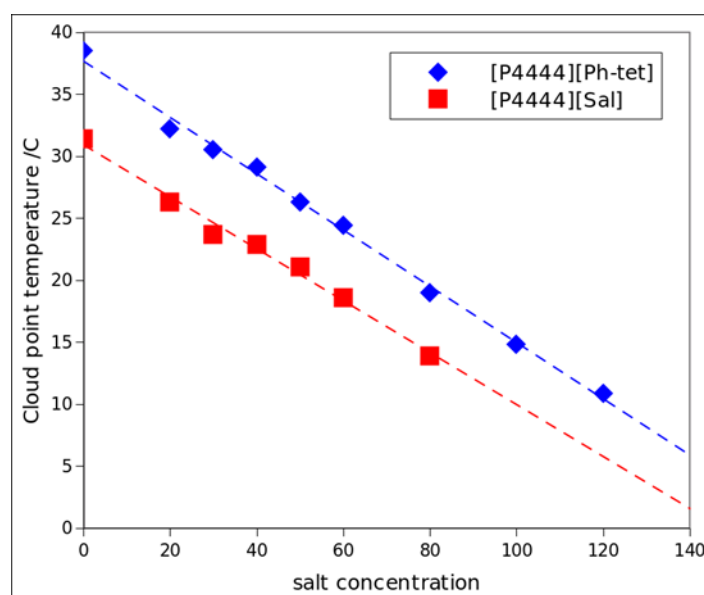


**Figure 3** - Comparison and contrast between  $[P_{4444}][Ph-tet]$  and  $[P_{4444}][Sal]$

### Conclusions and future work

The results identify the equation  $dT = aC^b$  from Patterson's group<sup>[1]</sup> which shows the relationship between salinity and phase transfer temperature. In these IL/water systems,  $dT$  is the change in cloud point (LCST) temperature,  $a$  is a constant relative to the salt used in the system,  $b$  is a constant of the binary system, and  $C$  is the salt concentration (in this system sodium chloride).

In the future work, we will develop and set up a lab-scale forward osmosis test system to test the performance of different ionic liquids draw solution and explore a biomass model to prove these effective ionic liquid draw solution.



## Reference

1. W. H. Patterson, *J. Chem. Soc., Trans.*, **1925**, 127, 2544-2549.

## QUILL Quarterly Report

November 2021 - January 2022

<b>Name:</b>	Yaoguang Song		
<b>Supervisor(s):</b>	Prof Peter Nockemann, Prof David Rooney (QUB), Dr Xiaolei Zhang (Strathclyde), Prof. Stuart Gibb and Dr Szabolcs Pap (UHI)		
<b>Position:</b>	PhD Student		
<b>Start date:</b>	3 <sup>rd</sup> Dec 2018	<b>Anticipated end date:</b>	31 May 2022
<b>Funding body:</b>	EU INTERREG VA Programme, managed by SEUPB		

## Thermochemical Conversion of Biomass Lignin into Mesoporous Carbon Materials

### Background

As a main component, lignin from biomass holds huge potential for producing mesoporous carbons (MCs)<sup>1,2,3</sup>, which represents upper-class valuable products amongst all lignin-based applications.<sup>4</sup> However, most preparation methods for MCs are empirical, leading to unpredictable topologic and structural properties thus likely unfavourable for aimed downstream applications. Soft-templating synthesis was reported successful to tune nanostructures effectively, but novel promising templates are still in need of development.

A good option is long-chain ionic liquids (ILs) comprised of solely ions, as they can form lyotropic liquid crystals (LLCs), micelles, and (micro) emulsions that have been used for templating synthesis as well. Besides, ILs are also increasingly seen in the dissolution and depolymerisation of lignin. Therefore, this programme aims to investigate the possibility to convert lignin into MCs by employing ILs as both structure-directing agent and solvent. The effective implementation involves both multiscale modelling for computational design of preparation method and tangible experimental validation.

In one of my previous quarterly reports, we introduced the coarse-grained (CG) molecular dynamics (MD) simulations to investigate the self-assembly of ternary mixtures containing IL template, phenolic compounds as precursor, and water as solvent. Computational work focused on two key factors that eventually determine the topological structures of porous polymer and carbon materials, which are the morphology of templates and the spatial correlation between precursor and the hydrophilic parts of the template.<sup>5,6</sup> Simulation results indicate that the precursors with varying hydroxyl groups influence both the morphologies of IL template and the distribution of phenolic compounds themselves. However, due to the impact of COVID-19 pandemic, experimental validation was only performed to verify the template-precursor spatial correlation using in-house NMR spectrometer. This report will summarise experimental results in the validation of morphologies of IL templates in ternary mixtures.

### Methodology

Small-angle X-ray Scattering (SAXS). SAXS experiments were recorded by the Offline DL-SAXS instrument Xeuss 3.0 (Excillum Ga MetalJet source, 9.2 keV,  $\lambda=0.71$  Å) in Diamond Light Source, Harwell Campus, Oxfordshire. The sample was transferred into a capillary (1.5 mm of outer diameter) and sealed tightly. Measurements were carried out under vacuum at variable

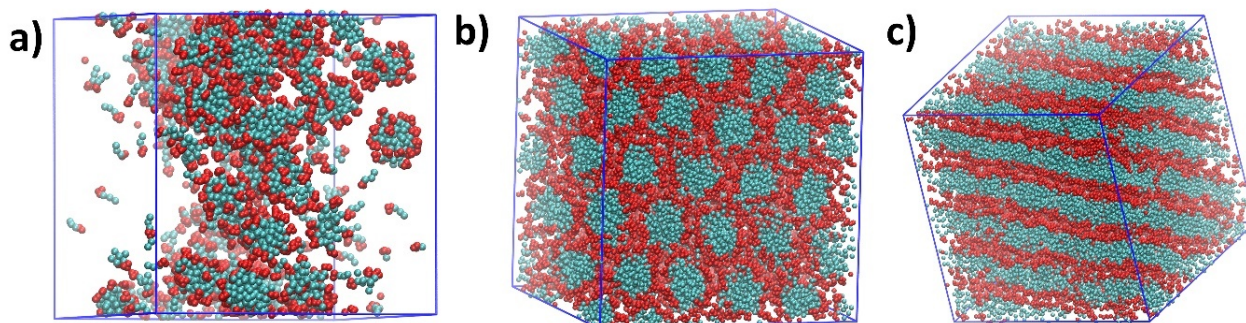


**Figure 1** - Snapshots of [C10MIM][OAc]/water/phenol ternary systems at water contents around: a) 50 wt%, b) 34 wt%, and c) 25 wt%. (Red and cyan beads represent imidazolium ring and alkyl chain of IL cation, respectively. Phenol, water, and anion are not shown for the ease of visualisation.)

temperatures with a detector to sample distance of 275 mm to ensure all possible characteristic peaks detected ( $q$  range 0.05-1.13  $\text{\AA}^{-1}$ ). An acquisition time of 300 s was used for all the samples. Data was corrected by subtraction of transmission and background scattering. The intensity was plotted versus scattering vector,  $q=(4\pi\sin\theta)/\lambda$ .

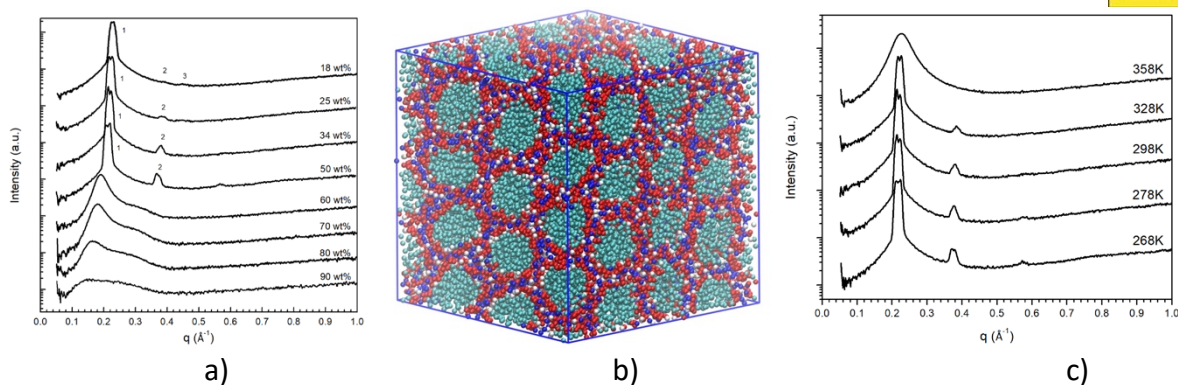
Polarised optical microscopy (POM). Phase examinations were performed under an Olympus BX50 microscope. All samples' textures were determined at 298.15 K with a Linkam TH600 hot stage and TP 92 temperature controller.

## Results

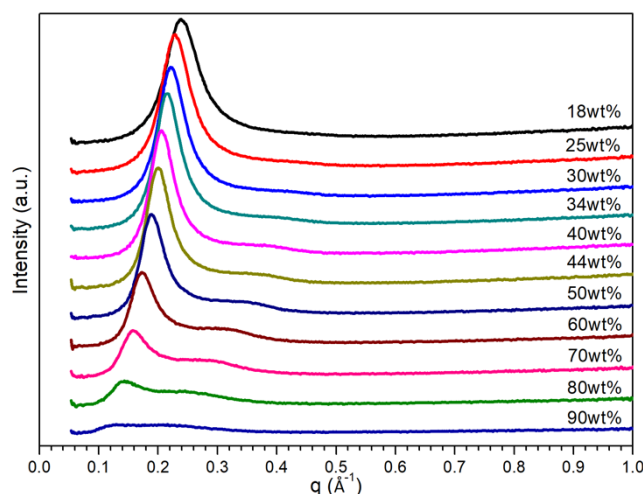
### 1) Influence of water content in the morphology of IL templates

Figure 1 shows three typical morphologies formed by  $[\text{C}_{10}\text{MIM}]^+$  cations in the presence of phenol as the precursor according to the CGMD simulation. With the decreasing water content (calculated based on IL and  $\text{H}_2\text{O}$  only, excluding phenolic precursor) in the mixture, spherical (at water content over 50 wt%), columnar (at water content between 29-44 wt%), and lamellar phases (at water content smaller than 25 wt%) formed sequentially once the IL concentration exceeded critical micelle concentration (CMC).

Small-angle X-ray scattering (SAXS) was performed for both  $[\text{C}_{10}\text{MIM}][\text{OAc}]/\text{water}$  binary and  $[\text{C}_{10}\text{MIM}][\text{OAc}]/\text{water}/\text{phenol}$  ternary mixtures to seek for experimental evidence. As shown in Figure 2a, the SAXS profiles of  $[\text{C}_{10}\text{MIM}][\text{OAc}]/\text{water}$  binary mixtures containing 18-50 wt% of water indicate the dominating hexagonal phase, evidenced by the characteristic scattering vector ratio  $q_1:q_2:q_3 = 1:\sqrt{3}:\sqrt{4}$ .<sup>7,8</sup> CGMD simulation also pointed out an ordered hexagonal structure when the water content reached 18 wt% (Figure 2b). Moreover, with the rise of temperature, these sharp characteristic scattering peaks become less intense even unobservable due to higher kinetic energy. Only a single broad  $q_1$  peak was detected for  $[\text{C}_{10}\text{MIM}][\text{OAc}]/\text{water}$  binary mixtures containing 34 wt% of water when temperature reached to 358.15 K (Figure 2c). At this point, the lyotropic mesophase were reversibly melt into an isotropic liquid phase and long-range liquid crystalline structures were disturbed, resulting in a dynamic short-range structural ordering of IL cations. This can be attributed that higher temperature brings increased kinetic energy, so the fixed liquid crystalline lattice was disrupted, leaving a dynamic short-range structural ordering.



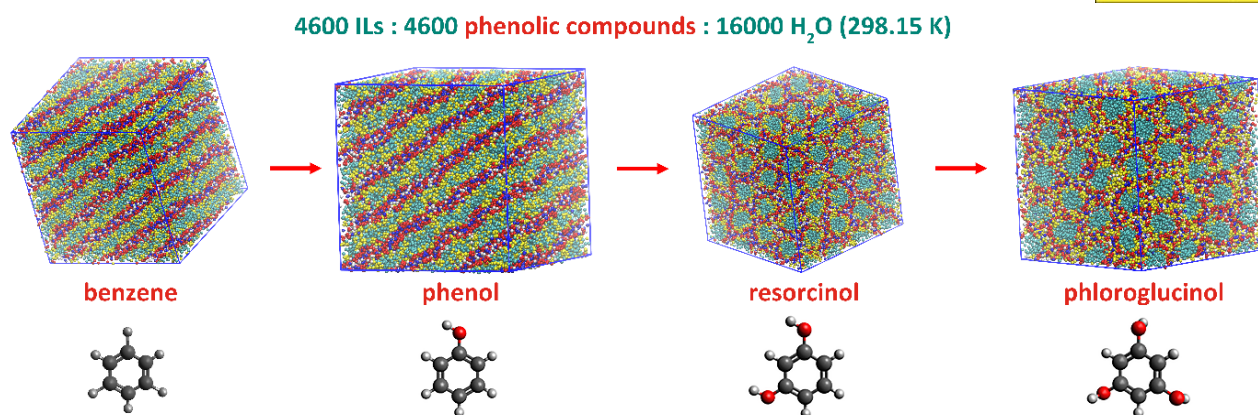
**Figure 2** - SAXS spectra of [C10MIM][OAc]/water binary mixtures with varying water contents at 25 °C; b) snapshot from MD simulation of [C10MIM][OAc]/water binary mixtures with 18.2 wt% of water; and c) SAXS spectra of [C10MIM][OAc]/water binary mixture containing 34 wt% of water at various temperatures



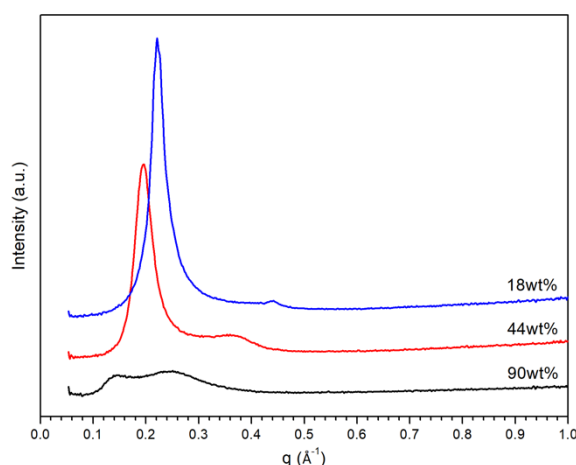
**Figure 3** - SAXS patterns of [C10MIM][OAc]/water/phenol ternary mixtures with varying water contents at 298.15 K

Figure 3 shows SAXS spectra for ternary mixtures containing phenol where only broad peaks were observed rather than sharp intense peaks. The SAXS profile for ternary mixture containing 18 wt% of water shows a single broad peak centred at  $0.24 \text{ \AA}^{-1}$ , which could be associated with the relative structural ordering in short-range. With the increase in water content from 30 wt%, the  $q_1$  peak gets lower and shifts to lower  $q$  range, while a second broad peak  $q_2$  gets higher and centred around  $0.38 \text{ \AA}^{-1}$ . When the water content exceeds 50 wt%, both peaks become weaker then merge into a much broader peak for mixture containing 90 wt% of water. Owing to the less intense nature of these scattering peaks, it is challenging to interpret morphological information for IL templates in ternary mixture. However, when the mixtures were quenched down to 263.15 K, more recognisable scattering peaks are manifested, which is probably because lower temperature results in slower molecule motion due to smaller kinetic energy. As shown in , two scattering peaks at  $0.22$  and  $0.44 \text{ \AA}^{-1}$  are observed for ternary mixture containing 18 wt% of water; the ratio  $q_1:q_2 = 1:2$  indicates the formation of lamellar bilayer array with a repeating distance  $d = 2\pi/q = 28.5 \text{ \AA}$ . At 44 wt% of water, a hexagonal phase is detected with a scattering vector ratio of  $q_1:q_2 = 1:\sqrt{3}$ . The broad peak observed from ternary mixture containing 90 wt% of water indicates that IL cations are dominantly assembled into spherical clusters.





**Figure 4** - Morphology evolution under increasing hydroxyl groups in phenolic compounds (Red: imidazolium ring, cyan: alkyl chain, blue: acetate anion, yellow: phenolic compounds, white: water)

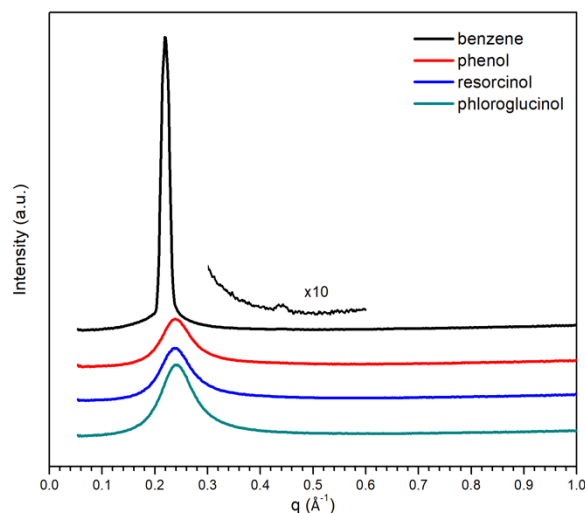


**Figure 5** - SAXS patterns of [C<sub>10</sub>MIM][OAc]/phenol/water ternary mixtures at 263.15 K

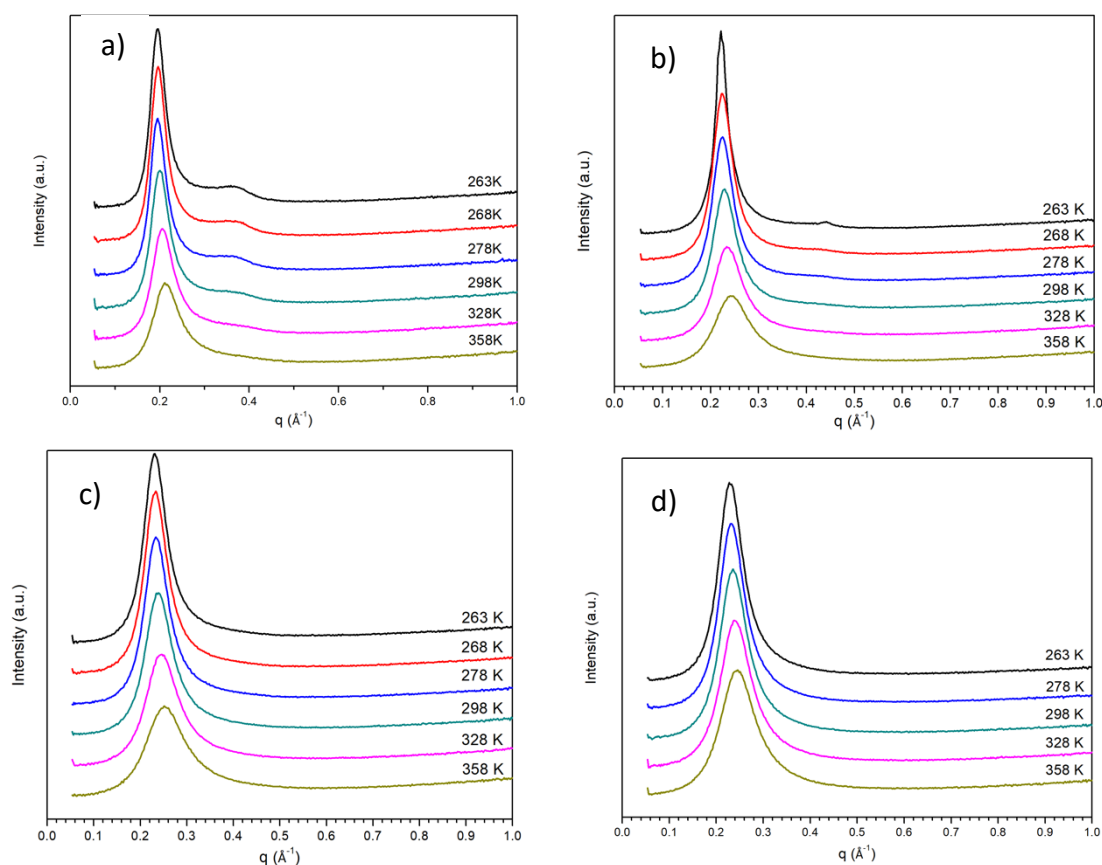
## 2) Influence of different precursors on the morphology of IL templates

Figure 5 shows the eventual configurations of ternary mixtures at 18 wt% of water. Benzene based ternary mixture also presents a planar lamellar phase like their phenol counterpart. In comparison with [C<sub>10</sub>MIM][OAc]/water binary mixture where dominating hexagonal columnar phase is observable, the addition of equimolar of phenol or benzene has changed the morphology of [C<sub>10</sub>MIM]<sup>+</sup> micelles. Most noticeably, when using resorcinol and phloroglucinol as precursors, the morphology of the [C<sub>10</sub>MIM][OAc] became hexagonal columnar, which is expected to appear at higher water contents for phenol-based cases. This indicates that the introduction of more hydroxyl functionalities also plays an analogous role as increasing water ratio in mixture. One hydroxyl functionality on phenolic compound can act as one H-bond donor and acceptor while per water molecule has double the capacity of phenol; phloroglucinol is able to form H-bonds quantitatively equal that of phenol “plus” water at maximum. This may lead to the morphological transition when using phloroglucinol to replace phenol. Figure 6 shows the SAXS profiles of IL/water/precursor ternary mixtures. Only broad peaks were observed for ternary mixtures, except that containing benzene where its scattering vector ratio  $q_1 : q_2 = 1:2$  signifies the presence of smectic lamellar phase. With the increase in hydroxyl groups, the broad scattering  $q_1$  peak gets stronger from ternary mixture containing phenol. The absence of the second scattering peak  $q_2$  makes it more challenging to interpret the morphological structures of [C<sub>10</sub>MIM]<sup>+</sup> cations in ternary mixture containing

resorcinol or phloroglucinol. Even at lower temperatures with smaller kinetic energies, unlike their phenol counterpart, there is still only one broad scattering peak observable (Figure 7).



**Figure 6** - SAXS spectra of ternary mixtures containing 18 wt% of water with different precursors: a) benzene, b) resorcinol, and c) phloroglucinol



**Figure 7** - SAXS profiles for ternary mixtures at various temperatures for different precursors: a) phenol at 34 wt% of water, b) phenol at 18wt% of water, c) resorcinol at 18wt% of water, and d) phloroglucinol at 18wt% of water.

POM was performed for ternary mixtures containing resorcinol and phloroglucinol. No lyotropic gels or LLCs were observed though hexagonal array obtained from CGMD simulation. The absence of



lyotropic gel did not apply to  $[C_{10}MIM][OAc]$ /water/benzene system, the cross pattern of which could be associated with the formation of lamellar phase (Figure 8a).<sup>7,9,10</sup> Liquid crystalline phase were also reported observable in  $[C_{16}MIM][Br]$ /water/p-xylene ternary mixtures.<sup>7</sup> This is because neither benzene nor p-xylene has functional moieties containing hetero-atoms to serve as H-bond donors and acceptors, therefore benzene and p-xylene are chemically stable in mixtures and unlikely to destabilise the H-bonding lattice between IL and water. However, when resorcinol or phloroglucinol were added in molar quantities less than  $[C_{10}MIM][OAc]$ , lyotropic gels were observed for ternary mixtures; the representative fan-like pattern exhibits the characteristics of hexagonal liquid crystalline lattice<sup>7,9,10</sup> (Figure 8b). This phenomenon confirmed that phenolic compounds compete with water to form H-bonds with ILs, particularly acetate anion. When ILs outnumber precursors, phenolic compounds are likely confined in dynamic hexagonal arrays *via* H-bonds with  $[C_{10}MIM][OAc]$  and water, and excessive  $[C_{10}MIM][OAc]$  form crystalline H-bonding lattice with water generating lyotropic gels on a macroscopic aspect. When resorcinol or phloroglucinol was added equimolarly with  $[C_{10}MIM][OAc]$ , the strong scattering  $q_1$  peak in their SAXS profiles could be resulted from the formation of hexagonal columnar arrays.

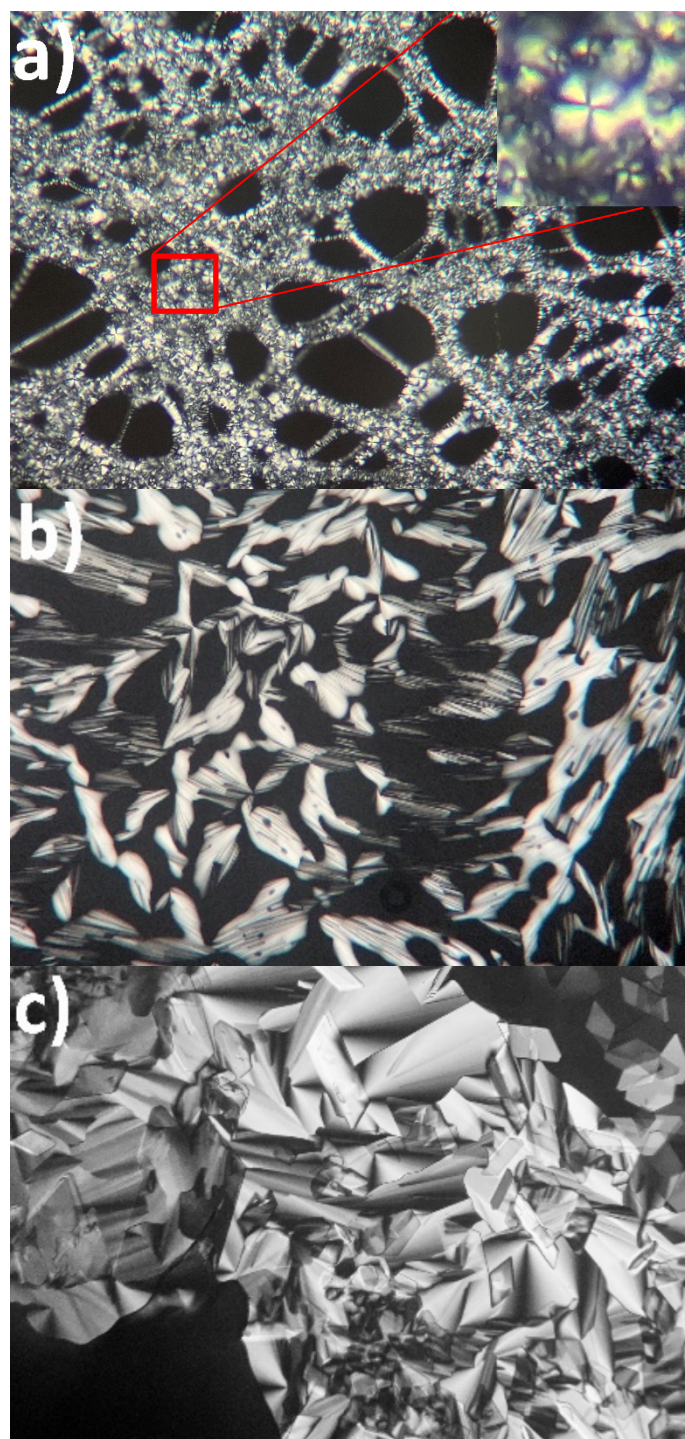


**Figure 8** - Representative POM images of lyotropic phase for ternary mixtures at around 18 wt% of water: a) ternary mixture containing benzene at  $[C_{10}MIM][OAc]/benzene$  ratio of 1:1; b)  $[C_{10}MIM][OAc]/water/resorcinol$  at  $[C_{10}MIM][OAc]/precursor$  ratio of 1:0.5; c)  $[C_{10}MIM][OAc]/water/phloroglucinol$  at  $[C_{10}MIM][OAc]/precursor$  ratio of 1:0.5

### Conclusions and future work

The SAXS and POM results on ternary mixtures confirmed that the morphology of IL templates can not only be controlled by the adjustment of water content in mixture but also the selection of different precursors.



In the future, we would focus on the templating synthesis of mesoporous carbons by employing IL templates, aiming to get porous carbon with IL templates recycled.

## References

1. D. Montané, V. Torné-Fernández and V. Fierro, *Chem. Eng. J.*, 2005, **106**, 1–12.
2. Y. Song, J. Liu, K. Sun and W. Xu, *RSC Adv.*, 2017, **7**, 48324–48332.
3. J. M. Rosas, R. Berenguer, M. J. Valero-Romero, J. Rodríguez-Mirasol and T. Cordero, *Front. Mater.*, , DOI:10.3389/fmats.2014.00029.
4. A. M. Puziy, O. I. Poddubnaya and O. Sevastyanova, *Top. Curr. Chem.*, 2018.
5. Y. Meng, D. Gu, F. Zhang, Y. Shi, L. Cheng, D. Feng, Z. Wu, Z. Chen, Y. Wan, A. Stein and D. Zhao, *Chem. Mater.*, 2006, **18**, 4447–4464.
6. D. Saha, R. Zacharia and A. K. Naskar, in *ACS Symposium Series*, 2014, vol. 1173, pp. 61–83.
7. J. Zhang, B. Dong, L. Zheng, N. Li and X. Li, *J. Colloid Interface Sci.*, 2008, **321**, 159–165.
8. N. Goujon, M. Forsyth, L. F. Dumée, G. Bryant and N. Byrne, *Phys. Chem. Chem. Phys.*, 2015, **17**, 23059–23068.
9. X. W. Li, J. Zhang, B. Dong, L. Q. Zheng and C. H. Tung, *Colloids Surfaces A Physicochem. Eng. Asp.*, 2009, **335**, 80–87.
10. T. Inoue, B. Dong and L. Q. Zheng, *J. Colloid Interface Sci.*, 2007, **307**, 578–581.



## QUILL Quarterly Report

November 2021 – January 2022

<b>Name:</b>	Richard Woodfield		
<b>Supervisor(s):</b>	Dr Stephen Glover, Dr Robert Watson and Prof Peter Nockemann		
<b>Position:</b>	PhD Student		
<b>Start date:</b>	06/2019	<b>Anticipated end date:</b>	12/2022
<b>Funding body:</b>	EPSRC		

### Modelling the use of Flow Batteries in Transport Applications

#### Background

Flow batteries have received significant attention in the past years for use in grid storage applications. The decoupling of the relationship between power and energy density offers a very unique way to store energy to suit the user's particular needs. The extremely long cycle life of a flow-battery is another attractive asset, as the electrodes do not undergo cyclic stressing in the same way Li-ion and other chemistries do. Flow-batteries have received very limited attention regarding their use in transport applications. There is untapped potential in the fact that the discharged electrolyte of a flow-battery could be rapidly swapped at a traditional gas-station, where the infrastructure is already half in-place with storage tanks under the stations. With the electrolyte being entirely re-usable, the station would use an on-site flow-battery to recharge their reservoir and provide passing vehicles with opportunity to swap their electrolyte with readily charged fluid.

#### Objective of this work

The overall goal of the project is to identify viable electric or hybrid modes of transport that would benefit from the use of a flow-battery, given the refillable nature of the flow-battery electrolyte reservoirs. Even the applications rendered not viable will have outcomes, as the amount by which the energy density of the electrolyte would need to improve by is also providing electrolyte chemists with targets to aim for. The investigations will be carried out using software to model battery and vehicle behaviour, primarily Simulink.

#### Progress to date

Modelling work has shown that coastal ferries are a very good candidate for RFB technology, and a paper has been submitted in this area.

#### Conclusions and future work

Modelling work is now shifting towards bus applications, exploring a range of system architectures and control strategies.

## QUILL Quarterly Report

November 2021 – January 2022

<b>Name:</b>	John (Mark) Young		
<b>Supervisor(s):</b>	Dr Leila Moura, Prof John Holbrey and Prof Sophie Fourmentin		
<b>Position:</b>	PhD student		
<b>Start date:</b>	2020	<b>Anticipated end date:</b>	2024
<b>Funding body:</b>	EPSRC		

### Gas separation technologies

#### Background

Biogas is a renewable and carbon neutral energy source obtained through anaerobic digestion (AD) of organic waste. Biomethane is obtained through the upgrading of biogas produced from anaerobic digesters. It consists of mainly methane and carbon dioxide with many trace compounds including hydrogen sulfide, ammonia, siloxanes, terpenes and water vapour. Biomethane must be of a purity equal to or better than that of natural gas if it is to be utilised for grid injection therefore a methane purity of above 96% must be achievable from any prospective technology. Carbon dioxide should make up 2.5-4% of the remaining volume with contaminants such as sulfur and siloxanes being limited to 10 mg/m<sup>3</sup> and 0.1 mg/m<sup>3</sup> respectively. The primary focus of this research is on carbon dioxide/methane separation as these are the two major components of biogas.

Currently biogas upgrading is multistep, with scrubbing used for carbon dioxide removal from the biogas stream to concentrate methane. This involves the use of liquid amines such as MEA (monoethanolamine) where carbon dioxide is captured through a chemisorption process. Regeneration of the amines requires high energy inputs in the form of steam at 100-150°C to reform the initial liquid amine. Water scrubbing can also be used but this requires large amounts of water and leads to methane slip due to the lower selectivity of water compared with other technologies. Membranes offer another option for upgrading but these also suffer from a range of issues such as a low throughput coupled with fouling and plasticisation. The degradation of membranes leads to issues both economically in the form of having to replace them but from an environmental standpoint it is unsustainable to continuously have to dispose of and manufacture replacement membranes. Cryogenic distillation offers a method of using nontoxic materials to produce high purity gas streams through the utilisation of low temperatures and high pressures which allows carbon dioxide to liquefy leaving a pure methane stream. However the energy cost associated with this method is massive which makes it less sustainable and exceedingly costly.

It is for these reasons that we seek to create novel materials which will be more efficient, more sustainable and economically viable. Initial work will consist of the use of deep eutectic solvents in conjunction with other sorbents to increase their upgrading capabilities.

#### Work to date

CO<sub>2</sub> uptake in TOPO-based hydrophobic low melting mixtures

The screening methodology has improved since previous reports with the utilisation of our own recently repaired head-space gas chromatograph (HS-GC). This has increased the maximum

screening pressure to around 3.5 bar, extending the scope from the upper limit of 1.8 bar as described in the previous report.

Hydrophobic low melting mixtures (HLMMs) have been a major focus of my research this quarter. They have been previously synthesised in QUILL based on trioctylphosphine oxide (TOPO) combined with acid hydrogen-bond donors (Fig 1) and have substantially lower viscosity than many other reported LMMs such as choline chloride based mixtures.<sup>3</sup>

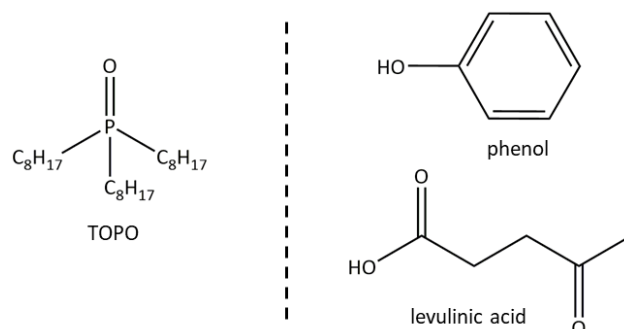


**Figure 1** - Structures of hydrogen bond acceptor (left) and hydrogen bond donor (right) components of TOPO-based HLMMs used in this work

Gas uptake measurements have shown that these materials have exceptionally high CO<sub>2</sub> uptake when compared with other DES physisorbants such as choline chloride:urea ([Ch]Cl:U) 1:2 as can be seen in Fig. 2 where the CO<sub>2</sub> uptake was ca. 2-3 times greater in the TOPO-phenol DES compared to the choline-based system. This has been attributed to the presence of the phosphine oxide group in the HLLM interaction strongly with CO<sub>2</sub> as has previously been seen in porous polymers but never before in LMMs.<sup>4</sup>

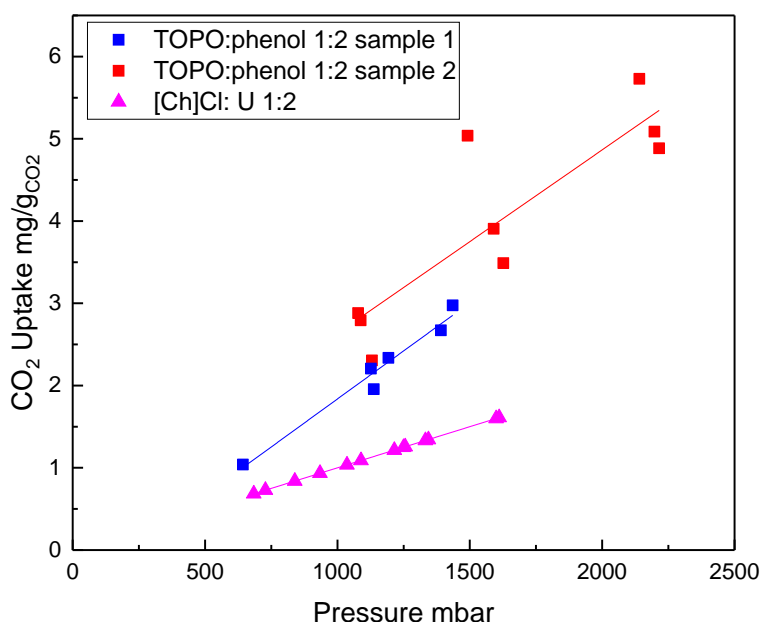


**Figure 2** - Plot of CO<sub>2</sub> uptake in mg/g as a function of pressure in TOPO: phenol 1:2 (red and blue) compared with [Ch]Cl:U (pink)



Due to the slight volatility and environmental concerns regarding the use of phenol, the HBD was then changed to the benign and cheaper natural product levulinic acid (Lev). The CO<sub>2</sub> uptake of this material can be seen below in Fig. 3, with an increase in uptake capacity over that measured for the TOPO:phenol 1:2 DES. TOPO:Lev was regenerated overnight under vacuum at 40°C which can be considered mild conditions. The uptake in CO<sub>2</sub> capacity however do not decrease substantially showing promise for this material over multiple absorption/desorption cycles.

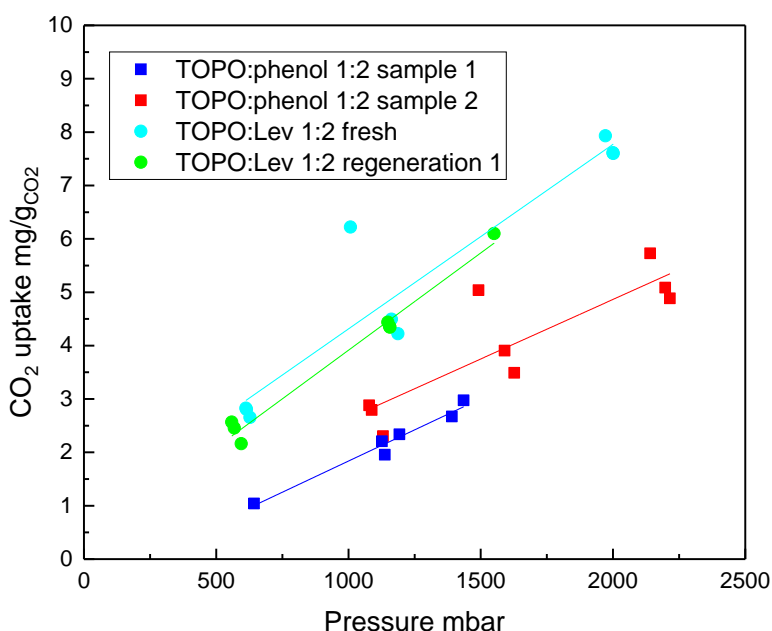


**Figure 3** - Plot of CO<sub>2</sub> uptake in mg/g as a function of pressure for of TOPO:Lev 1:2 and TOPO:phenol 1:2 LMMs

#### Inclusion of macrocyclic hosts to promote gas uptake

Protic ionic liquids (PILs) may offer a suitable environment to solubilise cucurbiturils (CBs) which are notoriously insoluble in traditional solvents. CBs have also been reported to have high CO<sub>2</sub> absorption capacities along with good selectivity over CH<sub>4</sub> through inclusion of CO<sub>2</sub> within the CB cavity. We have therefore attempted to combine these two characteristics, testing the potential to use PIL-CB composite materials as CO<sub>2</sub> sorbents.

Initial screening, as shown in Fig. 4, indicate that the solvation of 5 wt% CB in an acidic pyridine/sulfuric acid PIL (1:2 molar ratio) may increase the CO<sub>2</sub> capacity of the PIL. However, these first data sets show a large level of variability in CO<sub>2</sub> uptake and require further measurement to reduce the uncertainty and ensure reproducibility. It must be noted however that the increase in uptake capacity is significantly lower than that anticipated from complete filling of the available CB pores with CO<sub>2</sub> (absorption capacity of CB, 88 mg/g<sup>5</sup>) suggesting that the CB is not accessible and is competitively filled by solvent.

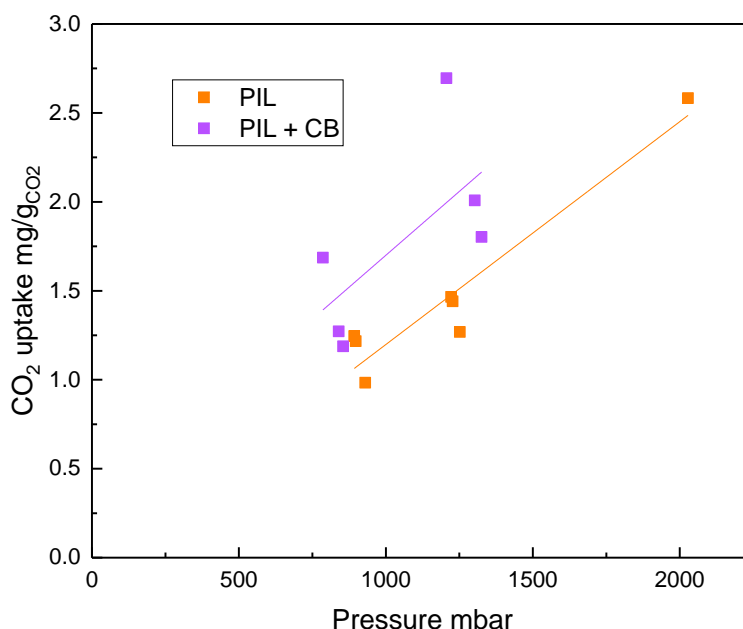


**Figure 4** -Plot of CO<sub>2</sub> uptake in mg/g as a function of pressure by pyridine/sulfuric acid 1:2 PIL (orange) and the same PIL containing 5 wt% dissolved CB (pink)

### Future work

Future work will be to test all the uptake capacities of the systems with pure CH<sub>4</sub> and with a 1:1 CO<sub>2</sub>/CH<sub>4</sub> (molar) gas mixtures to determine the CO<sub>2</sub>/CH<sub>4</sub> selectivity. This will give insight into their feasibility to be used for biogas upgrading and help elucidate gas adsorption mechanisms. NMR experiments will also be used in order to try to confirm the host guest chemistry between gas and macrocycles. Switching of phenol to a greener component such as catechol will also be tested in order to synthesise a more environmentally benign material while keeping the high capacity for CO<sub>2</sub>. Tests will also be carried out with dissolution of macrocycles in TOPO based DES.

Further testing will also be required to confirm if CB dissolved in PIL does increase CO<sub>2</sub> capacity as preliminary results have indicated, and the mechanism of interaction will be probed along with varying wt% of CB dissolved in PIL.

### References

1. F. M. Baena-Moreno, M. Rodríguez-Galán, F. Vega, L. F. Vilches and B. Navarrete, *Int. J. Green Energy*, 2019, 16, 401–412.
2. M. R. Rodero, R. Ángeles, D. Marín, I. Díaz, A. Colzi, E. Posadas, R. Lebrero and R. Muñoz, in *Biogas*, Springer, 2018, pp. 239–276.
3. E. L. Byrne, R. O'Donnell, M. Gilmore, N. Artioli, J. D. Holbrey and M. Swadźba-Kwaśny, *Phys. Chem. Chem. Phys.*, 2020, 22, 24744–24763.
4. S. Qiao, W. Huang, Z. Du, X. Chen, F.-K. Shieh and R. Yang, *New J. Chem.*, 2015, 39, 136–141.
5. H. Kim, Y. Kim, M. Yoon, S. Lim, S. M. Park, G. Seo and K. Kim, *J. Am. Chem. Soc.*, 2010, 132, 12200–12202.